Part I

Plasma science and technology

1

The physics and chemistry of plasmas for processing textiles and other materials

W. G. GRAHAM
Queen's University, Belfast, UK

1.1 Introduction

The unique physical and chemical characteristics of the plasma environment make it attractive for textile processing. A plasma is an ionised gas, i.e. it contains electrons, ions and neutral atoms and/or molecules. However, not all of the ionised gases used in textile processing will exhibit the properties associated with plasmas, mainly because of they have low charge state densities compared to the neutral gas density or are produced by transient phenomena. The physical characteristics of plasmas are described in this chapter, along with the general chemical characteristics and surface interactions of partially ionised gases. In Section 1.2 the basic properties of gases in which plasmas are created are introduced. Section 1.3 introduces the basic concepts of plasma creation and their physical structure, along with the conditions that must prevail for an ionised gas to behave as a plasma, and the parameters that describe the plasma. The unique aspects of plasma chemistry are described in Section 1.4 through discussions of the constituent species, their collisions and interactions. In textile processing, the interactions of the plasma generated species with and on the surfaces in contact with the plasma are of great importance and these are discussed in Sections 1.5 and 1.6, respectively.

1.2 Gases

The underlying neutral gas environment in the plasma systems used in textile processing can be quite complex and inevitably involves an initial mixture of atoms and molecules. The gas can be flowing and may have temperature and density gradients. However, the most useful approach to obtain a basic understanding of gas behaviour is through using kinetic theory. This approach makes the following assumptions: the gas consists of identical molecules; individual molecules are small compared to the average space between them; the molecules themselves are relatively

incompressible; and the molecules are in constant random motion. So here the gas will be assumed to be single species, uniformly distributed and not flowing. In addition, for simplicity, the term molecule will be used to describe all the neutral particles unless otherwise stated.

The continuous motion of the molecules is quantified in terms of their temperature. The higher the temperature, then the more vigorous is their average motion. Molecules acquire or lose energy through collisions with one another or through contact with solid objects. This energy is in the form of kinetic energy (E_K), related to the mass (M) and velocity (v) of the molecule by the expression

$$E_K = \frac{1}{2} M v^2 \qquad [1.1]$$

In a large population the molecules have a wide range of energies and the energy of an individual molecule is constantly changing. The energy distribution of such a collection of molecules is statistical and is described by a function known as a Maxwell–Boltzmann distribution The energy distribution can be defined by a single quantity, the temperature (T). The mean speed of molecules ($\bar{c}$) in such a gas is given by

$$\bar{c} = \sqrt{\frac{8kT}{\pi M}} \qquad [1.2]$$

where k is Boltzmann's constant = $1.38 \times 10^{-23}\,\mathrm{J\,K^{-1}}$, T is in Kelvin and M is the mass of the molecule in kg. So, for example, nitrogen molecules in air at 20 °C (293 K) have a mean speed of $500\,\mathrm{m\,s^{-1}}$.

In calculating the mean kinetic energy of the molecules in the gas, the mean square speed $\overline{c^2}$ is required, which for a Maxwell–Boltzmann distribution is given by

$$\overline{c^2} = \frac{3kT}{M} \qquad [1.3]$$

and therefore the average kinetic energy of the molecules is related to the gas temperature by the expression

$$\langle E_K \rangle = \frac{1}{2} M \overline{c^2} = \frac{3}{2} kT \qquad [1.4]$$

1.2.1 Mean free path

The moving molecules collide with one another. Between collisions, the molecules will travel in a straight line. Since the molecules are randomly distributed within the volume and are moving with different velocities, each one travels different straight line distances between collisions.

While $\bar{c}$ is the mean speed of the molecules, in collisions it is the relative mean velocity between molecules that is significant and this depends on the angle between the respective directions of motion of the molecules. It can be shown that for a Maxwell–Boltzmann velocity distribution and a uniformly dense gas, the mean velocity is $\sqrt{2}\bar{c}$.

If there are n_g gas molecules per unit volume, then the collision frequency (ν) or collision rate is given by

$$\nu = \sqrt{2} n_g \sigma_c \bar{c} \qquad [1.5]$$

where σ_c is known as the cross-section for the collision between the molecules. The cross-section is the effective area that a molecule appears to have when approached by another molecule. The concept will be discussed in more detail in Section. 1.4.3. As the temperature increases, the particle velocity increases and so therefore does the collision frequency.

The collision mean free path (λ_c) in such a gas is therefore

$$\lambda_c = \frac{1}{\sqrt{2}\sigma_c n_g} \qquad [1.6]$$

As the gas density increases, the mean distance a molecule moves between collisions decreases. The molecules in the air at atmospheric pressure and room temperature collide with each other with a frequency of about 10^9 collisions per second, with a mean free path between collisions of about 10^{-8} m. At 10 Pa, the mean free path increases to a few mm.

1.2.2 Particle flux and pressure

The particle flux (Γ) of a gas striking a unit surface or crossing an imaginary unit area from one side will depend on the velocity distribution of the gas molecules and the angular distribution of the molecular motion relative to the surface. Considering a static gas and molecules crossing the surface in a direction normal to the surface, it can be shown that

$$\Gamma = \frac{n_g \bar{c}}{4} \qquad [1.7]$$

Then

$$\Gamma = n_g \left(\frac{k_B T}{2\pi M} \right)^{1/2} \qquad [1.8]$$

i.e. the particle flux is directly proportional to the particle density and the square root of the gas temperature, and is inversely proportional to the square root of the mass of the molecules.

Pressure (P) is defined as the rate at which momentum is imparted to a unit area of surface. When a molecule bounces off a surface, there is a total change of momentum of $2M\bar{c}$ and so the rate of momentum change is $2M\overline{c^2}$. Molecules can be considered to be moving in six directions corresponding to the six faces of a unit cube, so on average $n/6$ molecules will cross a unit area in unit time. Therefore, from Equation 1.3

$$P = \frac{1}{3} M n_g \overline{c^2} = n_g kT \qquad [1.9]$$

1.3 Plasmas

A gas is normally an electric insulator. However, when a sufficiently large voltage is applied across a gap containing a gas or gas mixture, it will breakdown and conduct electricity. The reason is that the electrically neutral atoms or molecules of the gas have been ionised, i.e. split into negatively charged electrons and positively charged ions. The nature of the breakdown and the voltage at which this occurs varies with the gas species, gas pressure, gas flow rate, the materials and the nature, geometry and separation of the surfaces across which the voltage is sustained, the separation distance of the electrodes, the nature of the high voltage supply (e.g. dc, ac, radiofrequency or microwave) and the actual electrical circuitry.

The resulting ionised gas is often called a discharge or plasma. Those used in textile processing vary considerably but are usually only partially ionised gases containing electrons, ions and neutral atoms and/or molecules. The interactions of the electrically charged particles with each other, with the neutral gas and with contact surfaces produce the unique physical and chemical properties of the plasma environment. This environment is distinct from that found in solids, liquids or gases; hence plasmas are sometimes called the fourth state of matter.

A plasma is defined as a collection of positive and negative charges which act collectively. This implies that not only do the charges exert coulomb forces on each other but also that these forces are as important as, and dominate over, externally applied forces and effects due to collisions between themselves and any neutral gas present. In other words, the 'self-generated' electric fields play an essential role in how the particles move. A major consequence of this collective behaviour is the ability of the plasma to screen out local density perturbations and to create a sheath region between the plasma and contact surfaces. Not all ionised gases or discharges can be classified as plasmas; certain criteria must be meet before an ionised gas will exhibit the phenomena associated with a plasma's collective behaviour.

1.3.1 Electron and ion temperatures

A similar approach to the kinetic theory of gases can be applied to the electrons and ions in an ionised gases with energy and momentum exchange through collisions, albeit more complex than in a gas. However, the momentum transfer between the light electrons and the heavier gas molecules and plasma ions is not very efficient and often the energy deposition into the plasma favours the electrons. As a result, ionised gases, particularly at low gas pressures and charged particle densities, are described as non-thermal. This means that the constituents, e.g. the electrons, ions and gas molecules are each in thermal equilibrium only with similar mass species. The velocity distribution of each species can be represented by a Maxwell–Boltzmann distribution and the energy distribution quantified by a temperature. However, often the electron temperature is very considerably higher than the ion and gas temperatures, i.e.

$$kT_e >> kT_i \approx kT_g$$

where T_e is the electron temperature, T_i is the ion temperature and T_g is the gas temperature. In low pressure (<100 Pa) plasmas, the gas and ion temperatures can be 300 K while the electron temperatures may be over 20 000 K. In the literature, the temperature and other energies are often presented in terms of electron volts (eV), where

$$k\mathrm{T} = 1\,\mathrm{eV} \equiv 11\,600\,\mathrm{K}$$

The calculated Maxwell–Boltzmann energy distribution function for electrons with a density of $10^{16}\,\mathrm{m}^{-3}$ and temperature of 2 eV is shown in Fig. 1.1.

The mean speeds, mean free paths, collision frequencies and fluxes of electrons and ions can be calculated using the equations in Section 1.2 and the appropriate values for the electron and ion masses, temperatures and dominant collision cross-sections.

It is worth mentioning here that, in many low-pressure ionised gases, because of the electron heating mechanisms, inelastic collisions and the nature of the plasma, the electrons are not in thermal equilibrium and so their energy distribution is not represented by a Maxwell–Boltzmann distribution and cannot be defined by a temperature. This is discussed later.

As the electron-heavy particles collisions become more frequent, then the electrons transfer energy more rapidly and all the species approach the same temperature, so plasmas with high charged particle and gas densities are often described as thermal.

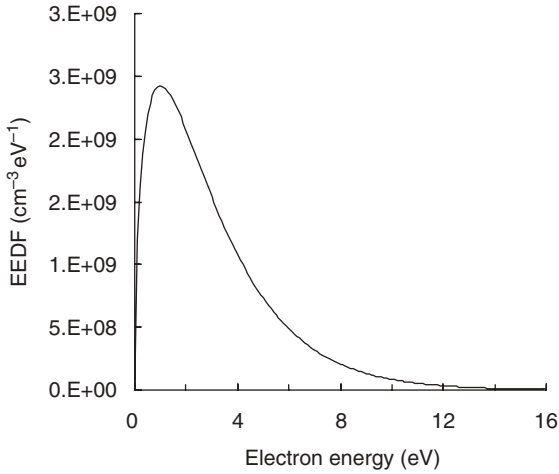

1.1 Calculated Maxwell–Boltzmann energy distribution function for an electron density of $10^{10}\,cm^{-3}$ at a temperature of 2 eV.

1.3.2 Quasineutrality

It is often stated that plasmas contain equal numbers of positively charged ions (n_i) and negatively charged electrons (n_e). The ionising events which maintain the plasma create an ion and electron pair and then the plasma self-sustains this charge equality. Consider a collection of these charges and then consider the removal of just one type, for example the electrons. Removing one electron leaves behind a net positive charge which will act to hold it back and removing more electrons results in a larger positive charge build up, making it increasingly harder to remove more electrons. So a great deal of energy is needed to separate the charges, and they consequently tend to stay together.

In fact, plasmas do not contain exactly equal numbers of electrons and ions, but the number of charges is huge and the difference is relatively small so we use the term quasi-neutrality and $n_e = n_i$ is a very good approximation.

1.3.3 Debye length

Plasmas act to screen out applied electric fields caused both by internal, localised inequalities in positive and negative charge densities and externally applied fields. Consider a quasi-neutral plasma and the introduction of a localised, enhanced electron density. The charge imbalance will generate a potential (ϕ), which will affect the surrounding ion and electron density. Since the electrons are much lighter than the ions, it can be assumed

that the ions are static. The electrons' response to the potential will depend on their kinetic energy, which, if they are in thermal equilibrium, can be expressed in terms of the electron temperature. The electron density at the perturbation is given by

$$n_e = n_\infty \exp(e\phi/kT_e) \quad [1.10]$$

where n_∞ is the undisturbed density far away from the negative charge perturbation. In one dimension it can be shown that the plasma acts to shield out the potential created by the perturbation so that at a distance x away the potential is given by

$$\phi = -\phi_0 \exp(-x/\lambda_d) \quad [1.11]$$

where λ_d has the dimensions of length, is called the Debye length and it is given by

$$\lambda_d = \sqrt{\frac{\varepsilon_0 kT_e}{e^2 n_e}} \quad [1.12]$$

where ε_0 is the permittivity of free space.

If we compare this potential around a charge in a plasma to the potential around a single 'naked' charge in a gas or vacuum (which falls off as $1/x$), we see that it falls off much faster in the plasma. The physical meaning of this is can be qualitatively understand. The charges in a plasma are in constant motion, but since like charges repel and opposites attract, each charge collects around itself a 'cloud' of opposite charge which screens out its field at large distances. This screening effect eliminates any large electric fields from the plasma and so $n_e = n_i$. Another result is that the plasma is spatially uniform meaning that large-area ionised gas regions can be formed. If plasma conditions do not prevail, then local charge density fluctuations can be amplified.

A practical formula for calculating the Debye length is

$$\lambda_d \approx 7400\sqrt{\frac{kT_e}{n_e}} \quad \text{(m)} \quad [1.13]$$

where kT_e is in eV and n_e is in m^{-3}.

If Debye screening is to be effective, then the typical ionised gas dimension (L_p) must clearly be larger than the Debye length. So $L >> \lambda_d$ is a plasma requirement.

1.3.4 Plasma parameter

The screening effects associated with the discussion of the Debye length are based on a statistical description of the electrons. This is valid only for

large numbers of particles. This can be expressed in the requirement that $N_D >> 1$, where N_D is the number of electrons contained in the Debye sphere, i.e.

$$N_D = n_e \frac{4}{3} \pi \lambda_d^3 \quad [1.14]$$

1.3.5 Plasma frequency

Any disturbance from quasi-neutral equilibrium will set up electric fields in a plasma. The electrons will move, in response to the fields, but as they accelerate they tend to overshoot the zero field position and oscillations are set up in the plasma. These oscillations occur at the plasma frequency (ω_{pe}) which can be written as

$$\omega_{pe} = \sqrt{\frac{e^2 n_e}{\varepsilon_0 m_e}} \quad [1.15]$$

where m_e is the electron mass. The plasma frequency is the natural 'ringing' frequency for the plasma. The electrons respond to an external disturbance on a time-scale given by the inverse of the plasma frequency.

A practical formula for the plasma frequency is

$$f_{pe} = \frac{\omega_{pe}}{2\pi} \approx 8.98\sqrt{n_e}\,(Hz) \quad [1.16]$$

where n_e is in m^{-3}.

While the lighter electrons dominate in the electric field screening, the ions also respond with a characteristic ion plasma frequency

$$\omega_{pi} = \sqrt{\frac{e^2 n_e}{\varepsilon_0 m_i}} \quad [1.17]$$

where m_i is the ion mass.

Collisions of electrons with gas molecules can damp these plasma oscillations, i.e. prevent them reacting with the time-scales required for collective behaviour. This requires that the electron collision frequency with molecules (ν_m) is less than the plasma frequency.

There are therefore three conditions for an ionised gas to behave as a plasma:

$$L_p >> \lambda_d \quad [1.18]$$

$$N_D >> 1 \quad [1.19]$$

$$\nu_m < \omega_{pc} \quad [1.20]$$

In a typical textile processing discharge, the electron densities are about $10^{16}\,m^{-3}$ and the electron temperature is about 2 eV. From Equation 1.13, the Debye length is the order of 0.1 mm; from Equation 1.14, $N_D \sim 4 \times 10^4$ electrons; and from Equation 1.16, the plasma frequency is in the microwave region (GHz).

The electron collision frequency, calculated using appropriate values in Equation 1.5, is considerably lower than the plasma frequency at low gas pressures (<100 Pa) but at atmospheric pressure it is much higher than the plasma frequency and deviations from plasma behaviour might be expected under those conditions. In addition, if, as in for example microdischarges or streamers, the ionising events occur over time-scales close to that of the plasma period (10^{-9} s), then again plasma behaviour is not expected and local charge density fluctuations can be amplified. These and other small dimension ionised gases might also not comply with the requirement that $L_p >> \lambda_d$.

1.3.6 Plasma structure and the sheath

In any textile processing application, the ionised gas will come into contact with a solid object. As well as the textile material, metal or dielectric-covered electrodes and chamber walls may be in contact with the plasma. If the ionised gas meets the criteria discussed above and can be characterised as a plasma, then potential structures will be created.

Initially, both electrons and ions move to the solid surface. The ion and electron fluxes can be determined from an equation similar to Equation 1.8. In the steady state, to maintain quasi neutrality, the ion and electron fluxes must of course be equal, but since the electron velocities are greater than the ion velocities and since their densities are equal, the electron flux at the plasma edge is greater than that of the ions. The plasma therefore self-adjusts to balance the loss rate of the ions and electrons. The positive charge left behind after the initial loss of electrons concentrates near the solid in a thin layer called the plasma sheath. This region is usually quite thin, is not quasi-neutral and so has potential gradients. These act to reflect electrons back into the plasma and accelerate the ions to the wall, creating a flux balance, so that in the plasma $n_i = n_e$ but in the sheath $n_i > n_e$. In many plasmas, the sheath can be seen as a thin, dark layer between a luminous region in the plasma and the contact surface. It is especially easy to see near electrodes that are driven with large voltages.

A result of the sheath creation and its associated electric fields is that the plasma is at a positive potential relative to any contact surfaces. This is known as the plasma potential. The magnitude of the plasma potential depends on a number of different parameters but clearly the ratios of the ion to electron masses and temperatures play a significant role. Similar

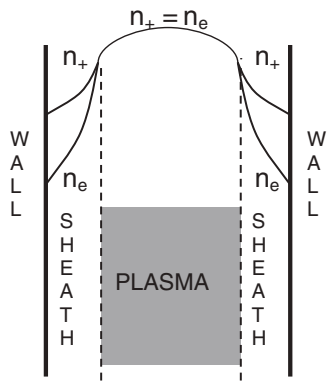

1.2 Plasma densities in a plasma and its sheaths.

arguments to those given above show that an electrically isolated object in the plasma will attain a negative potential relative to the plasma so as to balance the ion and electron flux. This is known as the floating potential.

The structure of a contained plasma is illustrated in Fig. 1.2. The quasi-neutral plasma is field free and sits at a positive potential relative to the grounded contact surfaces. Between the surface and the plasma is the sheath, a non-charge neutral region in which there is an electric field sustained by the potential gradient. This means that ions are accelerated towards the surface and therefore arrive with a kinetic energy determined by the plasma potential. This kinetic energy can be increased by biasing the contact surface so, depending on the operating conditions, ions with a well-defined energy, ranging from a few eV to keV, can be incident on the contact surface. In addition, any electrons produced at the surface or in the sheath region will be accelerated back into the plasma. This can be an efficient way of coupling energy into the plasma.

1.4 Plasma chemistry

1.4.1 Constituent species

Most processing plasmas are created in a molecular gas or a gas mixture that contains molecules. There are therefore a very large number of constituent species. The energy required to remove a single electron from a molecule or atom is known as the ionisation potential. The energies required to break molecules into various constituent parts are called the dissociation energies. As shown in Table 1.1, these are generally lower than the ionisation potential of the molecule and so there is often a high degree of dissociation in ionised gases. Dissociation products of the initial molecules are particularly important since they can be chemically reactive with the contact

Table 1.1 Energies characteristic of some atoms and molecules

Atom or molecule	Ionisation potential (eV)	Electron affinity (eV)	Metastable energy level (eV)	Lowest excitation energy (eV)	Dissociation energy (eV)
H	13.6	0.75		10.2	
He	24.6		19.8	21.2	
O	13.6	1.5	1.97	9.2	
F	17.4	3.5		12.7	
Cl	13.0	3.6		8.9	
H_2	15.6			11.5	4.5
O_2	12.5	0.45	1.2	7.9	5.1
Cl_2	13.2	2.5			2.5
C_6H_6	9.6				

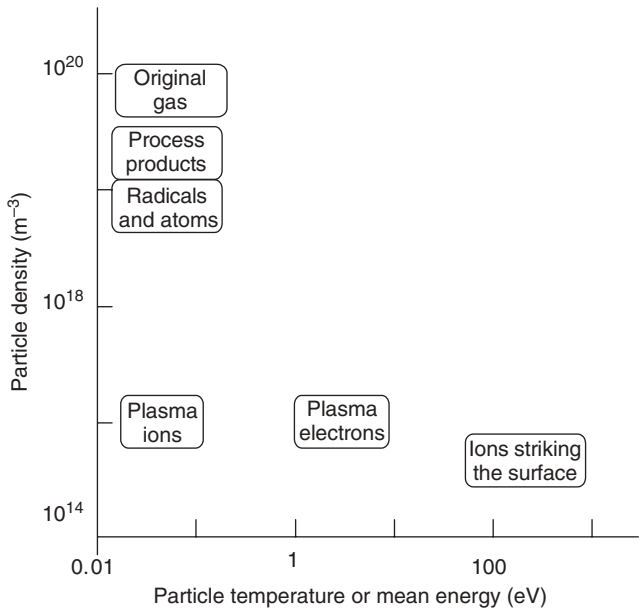

1.3 Densities and temperatures or energies for the constituent species in a typical low pressure plasma.

surfaces. In Fig. 1.3, the approximate densities and temperatures or energies of the plasma constituents in a typical low-pressure plasma are shown. Some atoms and molecules can accommodate an extra electron, so creating negative ions; the stability of such negative ions can be gauged from their electron affinity and some values for these are shown in Table 1.1.

In addition, the electronic structure of the constituent atoms and molecules may be temporarily excited from its lowest (ground state) configuration to a higher energy, excited state level, usually in a collision with an electron. The additional energy is then released by the emission of light, generally in tens of nanoseconds or less, as the atom or molecule returns to its ground state. This light emission ranges from the infrared red to the vacuum ultra violet and can also produce chemical changes on the contact surfaces. However, sometimes the atomic or molecular excited state has an electronic structure that delays the light emission for up to a few seconds. These are called metastable states and they can play an important role in plasma initiation and plasma chemistry.

The constituent atoms of the molecules are not at rest but are in constant motion, both rotating around a common centre of mass and vibrating along their common axes. This rotational and vibrational motion has a lowest energy state; energy transferred to the molecule in collisions can increase the level of rotational and vibrational excitation of the molecule. The energy level differences are typically only about 0.001 to 0.01 eV for rotational states and 0.1 to 0.4 eV for vibrational states. The behaviour of the molecule in a collision can be influenced by its level of rotational and vibrational excitation since high ro-vibrational states can be excited with total energies of up to several eV.

1.4.2 Collisions

Just as in a neutral gas, as discussed in Section 1.2, the moving charged and neutral particles are colliding or interacting and reacting. The presence of energetic charged particles, particularly the electrons, lead to unique plasma chemistry. There are a huge number of interactions that can take place, particularly in a molecular plasma. In each collision, momentum and energy must be conserved. The collisions can be broadly classified into three types:

(i) Elastic collisions in which the momentum is redistributed between the colliding particles; the incident particles change direction but their total kinetic energy remains unchanged.
(ii) Inelastic collisions in which the momentum is redistributed between the colliding particles but where some fraction of the initial kinetic energy is transferred to the internal energy of one of the participating particles. This leads to the dissociation, excitation or ionisation of one or both of the participants.
(iii) Superelastic collisions in which the momentum is redistributed between the colliding particles and where the internal energy from one or both of the participants is transferred to the final total kinetic energy of the participants.

Table 1.2 lists some of the important types of reactions that occur in plasmas where most of the collisions involve only two particles. At higher pressures, collisions involving three bodies become probable. This allows even more diversity of reactions since the third body takes away momentum and allows reactions not physically possible between the other two bodies to occur. The third body can be another atom, molecule, electron or a surface. In some apparent two-body collisions, an emitted photon can take on the role of a third body.

As mentioned previously, some atomic or molecular states may be long-lived. These metastable states usually make a collision before they radiate, transferring their electronic energy to another constituent of the plasma. This energy may be enough to ionise a neutral atom or molecule with a lower ionisation potential in the collision. This is called Penning ionisation. Inert gases have particularly high energy, long-lived metastable states. The

Table 1.2 Some of the possible reactions of plasma constituents in the plasma volume

Reaction type	Name	
Electron impact	Ionisation	$e + A \rightarrow 2e + A^+$
	Dissociation	$e + AB \rightarrow e + A + B$
	Dissociative ionisation	$e + AB \rightarrow 2e + A + B^+$
	Dissociative attachment	$e + AB \rightarrow A^- + B$
	Electronic excitation	$e + A \rightarrow e + A^*$
	Ro-vibrational excitation	$e + AB \rightarrow e + AB$ (v, j ≥ 1)
	Momentum transfer	$e + A \rightarrow e + A$
Neutral	Dissociation	$AB + M \rightarrow A + B + M$
	Penning Ionisation	$Am + B \rightarrow A + B^+ + e$
	Atom transfer	$A + BC \rightarrow AB + C$
	Rearrangement	$AB + CD \rightarrow AC + BD$
	Recombination	$A + B + M \rightarrow AB + M$
	Energy transfer	$A^* + B \rightarrow A + B^*$
	Relaxation	$A^* + B \rightarrow A + B$
	Momentum transfer	$A + B \rightarrow A + B$
Ion	Neutralisation	$A^- + B^+ \rightarrow A + B$
		$A^- + BC^+ \rightarrow AB + C$
	Associative detachment	$A^- + B \rightarrow AB + e$
	Charge transfer	$A^+ + B \rightarrow A + B^+$
		$A^- + B \rightarrow A + B^-$
	Dissociative charge transfer	$A^+ + BC \rightarrow A + B + C^+$
	Momentum transfer	$A^+ + B \rightarrow A^+ + B$

Note that e represents electron, * an electronically excited state, v and j the vibrational and rotational quantum numbers, respectively, A*m* a long-lived metastable state and M indicates any molecule and indicates third-body stabilisation.

metastable states represent a storage of energy within the atoms or molecules and they can play an important role in the kinetic behaviour of plasmas. Vibrationally and rotationally excited states often have long lifetimes, and although the total energies involved are generally less than for atom metastable states, they can also act as an energy reservoir in the plasma and can, for example, influence the electron temperature through superelastic collisions.

1.4.3 Cross-sections and reaction rates

Collision cross-sections (σ_c) quantify the probability of a collision taking place between two or more particles. For two bodies in collision this represents the effective area of a particle as seen by another passing particle. This is unique to any pair of particles; for example, the interaction between two charged particles will be stronger than that for two uncharged particles and so the cross-section will be larger. The strength of the interaction between the two particles will also depend on the length of time for which they interact, i.e. their relative velocity or energy. There may also be threshold energy for a reaction to be possible, e.g. from Table 1.1, for the ionisation of a molecule (O_2) by an electron, the kinetic energy in the collision must at least be equal to the ionisation potential of the molecule (12.5 eV). Information about cross-sections for the many diverse reactions in a plasma is essential for an accurate insight into the plasma chemistry. Unfortunately, in many cases the data are sparse. However, the pervasive use of fluorocarbon plasmas in the microelectronics industry means that there are some quite comprehensive databases. Figure 1.4 shows some of the energy dependences of cross-sections for a wide range of collision processes in CF_4 but which are typical of the type of collisions in molecular plasmas.

1.4.4 Reaction rates

The number of collisions between two particle species (*1* and *2*) per unit time per unit volume (R_{12}) depends on the number density of both species, the cross-section and the time taken for the particles to move from one potential collision to the other, which in turn depends on their relative velocity (v), i.e.

$$R_{12} = n_1\, n_2\, \sigma_c(v)v \qquad [1.21]$$

As discussed earlier, in a plasma, the particles have a distribution of velocities, more often expressed as their energy distribution. The plasma chemistry pathways are frequently initiated by electron collisions. Equation 1.21 is therefore often written as

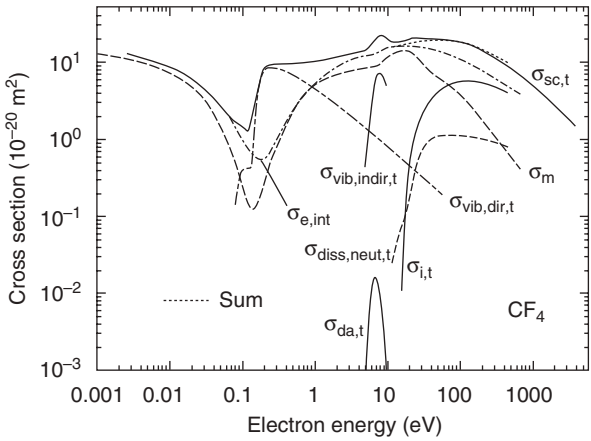

1.4 Energy dependence of cross-sections for electron collisions with CF_4. The notation refers to inelastic collisions (e,int), vibrational excitation (vib), dissociation of neutral molecules (diss,neut), inelastic dissociative attachment (da) etc. t refers to theoretical calculations. (from Christophorou, L.G. and Olthoff, J.K. (2002), *Applied Surface Science*, 192, (1–4), 309–326).

$$R_{12} = n_1\, n_2 <\sigma_c(v)v> \qquad [1.22]$$

where $<\sigma_c(v)v>$ is a mean value over the velocity distribution for a given temperature, is often written as K the rate constant and has units of area times velocity, e.g. m^3s^{-1}. These rate constants have different functional dependences on temperature because of the different energy dependences of the collision cross-sections, as illustrated in Fig. 1.4.

1.5 Plasma–surface collisions

The collisions of the plasma constituent species with the contact surface are the most significant interaction in materials processing applications. The plasma can deliver *kinetic energy* through ions accelerated in the sheaths and by vibrationally excited molecules, *potential energy* through the charged ions and metastable states, *chemical energy* through plasma-produced reactive atoms and radicals and *electromagnetic energy* (light) from the decay of electronically excited species. The interaction with the surfaces is complex and many different processes can occur; a few important ones are listed in Table 1.3. Since there has been no detailed studies of specific plasma–textile surface interactions, the following discussion will mainly focus on defining the various interactions which have been studied for solid surfaces and which may affect exposed textile surfaces.

Table 1.3 Some of the collisions and reactions of the plasma constituents with a surface

Reaction type	Name	Reaction
Neutral	Adsorption	$A + (s) \rightarrow A(s)$
	Desorption	$A(s) \rightarrow A + (s)$
	Dissociative adsorption	$AB + (s) \rightarrow A(s) + B(s)$
	Associative desorption	$A(s) + B(s) \rightarrow AB + (s)$
	Reaction at surface	$A + B(s) \rightarrow AB(s)$
	Reaction on surface	$A(s) + B(s) \rightarrow AB(s) + (s)$
	Electron emission	$A_m + (s) \rightarrow A(s) + e$
Ion	Neutralisation	$A^+ + e(s) \rightarrow A + (s)$
	Sputtering	$A^+ + e + B(b) \rightarrow A + B$
	Assisted desorption	$A^+ + e + B(s) \rightarrow A + B + (s)$
	Enhanced etching	$A^+ + e + B(s) + C(b) \rightarrow A + BC + (s)$
	Incorporation into bulk	$A^+ + e \rightarrow A(b)$
	Electron emission	$A^+ + (s) \rightarrow A(s) + e$

Note that e represents an electron, (s) an open surface site, A(s) a species A bound to the surface, B(b) a B species in the bulk and A*m* a long-lived metastable state.

1.5.1 Ion impact

At low ion energies, <15 eV, the ions lose energy and exchange momentum with the outermost atomic layers. Here, the potential energy of the ion, through its ionisation potential, plays an important role and at metal and semiconductor surfaces. The incoming ions can also be entrapped inside the solid if their kinetic energy is entirely dissipated in collisions with the atoms of the solid. As the energy increases, the penetration depth increases and so too does the entrapment. This can be strongly influenced by the porosity of the surface, with channels, etc. enhancing the trapping.

Ions striking a surface with energies above about 15 eV can remove atoms from the surface. This process is known as sputtering and it plays a key role in many plasma deposition and etching processes. Sputtering results from the transfer of kinetic energy and momentum from the incident ion to the atoms in the solid. If enough momentum is transferred to an atom in the direction of the surface, so that it has sufficient kinetic energy to overcome its surface binding energy, then that atom will be liberated (sputtered) from the surface. The number of particles sputtered per incident particle is very sensitive to the ion energy, the ratio of the masses of the incident and target particles, and the properties of the solid and surfaces. For metals, at around 30 eV only one atom is sputtered for every one thousand incident ions, but this increases to one atom for each incident ion at about 1 keV.

Atoms interacting with surfaces at these energies behave in a similar way to ions, since the ions are neutralised as they approach the surface. Relatively

small neutral and ionic molecules (<6 atoms) approaching the surface will exhibit similar behaviour to atoms and atomic ions at the same energy. However, each atom can appear to interact separately and locally with the surface and with a total kinetic energy that is the ratio of its mass relative to the number of constituent atoms of the molecule. This means that molecules generally require higher energies than atoms and atomic ions to produce the same effect. Large molecules will dissipate their energy over very many surface atoms and their energy can usually be accommodated within the lattice of the solid and so have little effect. Molecules also bring energy to the surface in the form of their rotational and vibrational excitation.

As well as the reflection and sputtering of incident atoms and ions, particle impact can also produce electrons, particularly at metal electrode surfaces. These are accelerated into the plasma by the sheath potential and so they can play a very important role in sustaining the plasma. There are a number of different processes that can lead to electron production. On metals, if the ionisation energy of the atom of an incident ion is twice the work function of the surface, then an electron can be emitted by a process called potential emission, but this is not significant on insulating surfaces. There is also kinetic emission of electrons from solids resulting from the ionisation of the atoms in the solid by the transfer of energy from the rapidly moving incoming ions or atoms. If an electron is produced with sufficient energy, it can escape through the solid to and beyond the surface. This therefore requires comparatively high-energy incoming particles and the threshold ion energies for metals are generally around 1 to 2 keV. The yield around threshold is less than about 0.05 electrons per incident particle. However, kinetic electron emission yields from insulating and semiconductors are generally higher than those from metals and the thresholds energies are a few hundred electron volts. The photoelectric emission of electrons as a result of plasma light emission is often ignored but it is thought to play a significant role in the development of some high-pressure arcs and microdischarges.

1.5.2 Atom and molecule reactions

The atoms, molecules and radicals will arrive at the surface with a thermal distribution of energy which in most textile processing plasmas will be just above room temperature. They react both with and on the surfaces.

Absorption

Atoms, molecules and radicals can be adsorbed due to an attractive force between an incoming molecule and a surface. If it is Van der Waals force,

produced by an electrostatic attraction caused by a mutual polarisation of two interacting atoms, then this is known as physisorption. This is a weak interaction with the bond energies between about 0.01 and 0.25 eV.

If a chemical bond is formed, i.e. there is a sharing of valence electrons by the interacting atoms, this is known as chemisorption and the energies are those associated with chemical bonds, i.e. from about 0.4 to 4 eV.

The incoming atoms and molecules that stick to the surface are termed adsorbates. If A is the incoming atom and S is the surface, both adsorption phenomena can be represented by the following reaction

$$A + S \rightarrow A{:}S \qquad [1.23]$$

An incoming molecule ($A{=}B$) with multiple (double, triple, etc.) bonds can be chemisorbed by the breaking of one of its bonds, e.g.

$$A{=}B + S \rightarrow AB{:}S \qquad [1.24]$$

while single-bonded molecules are often dissociated as they are bound to the surface

$$AB + S \rightarrow A{:}S + B{:}S \qquad [1.25]$$

This requires that there are two sites available on the surface and is known as dissociative chemisorption.

Not all atoms or molecules incident on the surface are adsorbed. The sticking coefficient (s) is defined as the flux of molecules that are adsorbed (Γ_{ads}), over the flux of molecules incident onto the surface (Γ_A), and from Equation 1.7

$$\Gamma_{ads} = s\Gamma_A = \frac{1}{4} s n_{AS} \bar{c}_A \qquad [1.26]$$

where n_{AS} is the gas density close to the surface and $\bar{c}_A$ is the mean atom or molecule speed.

In general, s depends on the relative reactivity of the incident atom or molecule with the surface, the gas temperature and the fraction of the possible sites on the surface that the incident atom or molecule can occupy. Generally, chemisorption only occurs until all the available sites on the surface are occupied, i.e. there is a monolayer of adsorbate molecules or atoms on the surface. Further absorption is by the much weaker physisorption.

Desorption

Desorption is the reverse reaction to adsorption and so can be written as the reaction

$$A{:}S \rightarrow A + S \qquad [1.27]$$

In thermal equilibrium, adsorption and desorption are in balance. Associative desorption is the reverse of dissociative adsorption.

$$2A{:}S \rightarrow A_2 + 2S$$

or $$A{:}S + B{:}S \rightarrow AB + S \qquad [1.28]$$

1.5.3 Surface kinetics

As with plasma chemistry, the relative probability that particular processes will happen can be described in terms of rate constants (K). Figure 1.5 considers a plasma in contact with a surface with which it can react chemically; the reactive atoms or molecules flow from the plasma, arriving at the surface at a rate (K_a), where they are adsorbed (K_b) and react chemically (K_c) to produce some product, which then desorbs (K_d) and flows into the gas phase (K_e). Alternatively, the reactive atoms may desorb without undergoing any reaction (K_f) or may undergo associative desorption with a reactive atom already on the surface (K_g). Finally the reaction products in the gas phase can return to the surface (K_h).

Consider the reaction of an atom A with a surface S. It can be adsorbed and subsequently desorbed.

$$A + S \underset{K_d}{\overset{K_a}{\leftrightarrow}} A{:}S \qquad [1.29]$$

If n'_0 is the area density (m^{-2}) of available adsorption sites for A on the surface S and $n'_{A:S} = n'_0\theta$ is the area density of sites covered with adsorbed molecules ($m^{-2}s^{-1}$). (Note: $'$ is used to indicate an area density rather than a volume density.) Then the flux of A adsorbing onto the surface is

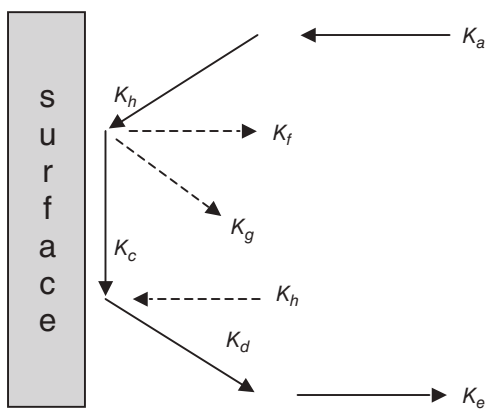

1.5 Schematic of the processes that can occur when a reactive species interacts with a surface.

proportional to the fraction of sites not covered with adsorbate, i.e. $1 - \theta$, so the flux of atoms adsorbing to the surface is

$$\Gamma_{ads} = K_a n_{as} n'_0 (1 - \theta) \quad [1.30]$$

where K_a is a second order rate coefficient.

In equilibrium this will equal the flux of atoms desorbing from the surface

$$\Gamma_{desorb} = K_d n'_0 \theta \quad [1.31]$$

where K_d is a first-order rate coefficient.

$$\theta = \frac{\frac{K_a}{K_d} n_{as}}{1 + \frac{K_a}{K_d} n_{as}} \quad [1.32]$$

i.e. if the adsorption and desorption rates and the gas atom density are known, the coverage of atoms on the surface can be calculated.

1.5.4 Plasma chemistry: Some unique features

The simple analysis presented above ignores the complexity of the plasma environment, where there are many different atomic and molecular, and neutral and charged, species incident on the surface. The microelectronics industry has used plasma phenomena with great effect, e.g. to obtain material selectivity and complex etch profiles. While the processes developed there may not be directly applicable to textile processing, some of the concepts and techniques might well find application. Examples are the use of gas mixtures to control surface reactions, balancing deposition and etching rates, and using the physical sputtering by the sheath accelerated ions, synergistically with surface chemical reactions.

1.6 Summary

There is an increasingly wide variety of approaches to generating ionised gases for textile processing. The primary motivation is to be able to generate specific reactive species from relatively inert feedstock gases. In ionised gases, and particularly in plasmas, these reactive species can be produced by energetic electron collisions with molecular precursors. Since the momentum transfer between the light electrons and the heavier gas molecules and plasma ions is not very efficient, as a result in plasmas, this highly reactive chemistry can be created in an environment where the ion and gas temperatures remain close to room temperature particularly at low gas pressures and charged particle densities.

A plasma is defined as a collection of positive and negative charges which act collectively. This implies that not only do the charges exert coulomb forces on each other, but also that these forces are dominant over, externally applied forces and effects due to collisions between themselves and any neutral gas present. A major consequence of collective behaviour is the ability of the plasma to screen out local density perturbations and to create a sheath region between the plasma and contact surfaces. Ions which diffuse through the plasma to the sheath edge are accelerated towards the surface. This delivers additional kinetic energy to the surface, along with the flux of reactive species, and can be used for process selectivity.

However, not all ionised gases or discharges can be classified as plasmas. Certain criteria must be meet before an ionised gas will exhibit the phenomena associated with plasma collective behaviour.

The criteria used in defining a plasma have been presented, along with the potential structure of the plasma and the electron-collision dominated plasma chemistry. The interaction of the plasma-created species with the contact surfaces has been described.

There is much unknown about the underpinning plasma physics and chemistry aspects of textile processing. The dominant role that plasmas have held in the microelectronics industry has driven much of the research to date and most of our basic ideas on low-pressure plasma processing of textiles derives from that work, but it may be inappropriate. Sheath formation near textile materials' surfaces has still to be explored. Also the required chemistry is very different and often more subtle, so for example the effect of charged particle bombardment and plasma light emission on the textile surface chemistry has yet to be resolved. The underpinning plasma and surface chemistry of the precursor gases of interest is still in its early stages.

There is a huge interest in using atmospheric-pressure ionised gases in textile processing. Here, the ionised gas may not be a plasma; however, there may be important exceptions, e.g. atmospheric-pressure glow discharges. There is still much to be done to understand the physics and chemistry in this revitalised area of high-pressure, non-thermal ionised gases.

1.7 Bibliography

Glow Discharge Processing, B. Chapman (John Wiley & Sons) 1980. This is a very good beginning level entry point for scientists and engineers interested in the field of low-pressure ionised gases, sources and surface interactions. It is focused largely on aspects of interest to the microelectronics industry.

Principles of Plasma Discharges and Materials Processing (Second Edition), M.A. Lieberman and A. Lichtenberg (John Wiley & Sons) 2005. This book provides a

very comprehensive and technically detailed account of the underlying science of low-pressure plasma processing, again orientated to the interests of the microelectronics industry.

Industrial Plasma Engineering (Volumes 1 & 2), J.R. Roth (Institute of Physics Publishing) 1995 and 1997. These two ambitious volumes cover the complete spectrum of industrial plasma science and technology from fundamental plasma physics to the engineering details of plasma sources at both low and high pressure.

Non-equilibrium Air Plasmas at Atmospheric Pressure, Editors: K.H. Becker, U. Kogelschatz, K.H. Schoenbach and R.J. Barker (Institute of Physics Publishing) 2005. This is a very comprehensive, detailed review of high-pressure non-equilibrium plasmas covering both the underlying science and technology.

2

The diagnosis of plasmas used in the processing of textiles and other materials

J. W. BRADLEY AND P. M. BRYANT
University of Liverpool, UK

2.1 Introduction

Plasma diagnostic tools are an essential element towards the proper understanding and development of technological plasmas. Knowledge of the particle densities and energies in the bulk and at boundaries, the electrical potentials and the spatial and temporal evolution of these parameters allow technologists to operate plasmas in the most efficient way and allow the intrinsic plasma processes to be tailored to suit a particular application.

There are many different diagnostic tools that can be used, depending on the type of plasma under investigation and the specific information that is required. Here, we have chosen to highlight four techniques frequently used in both academia and industrial settings. The first of these is the interpretation of the driving current and voltage waveforms. These measurements do not affect the plasma and can yield useful information on the major processes in the discharge. The second is electrical probing which, by their nature, are intrusive, since their presence affects the plasma under investigation. Their use is usually confined to low-pressure and low-temperature plasmas in which the heat flux will not destroy the integrity of the probe. The third area is mass spectrometry, which is most often performed at the substrate or plasma boundaries and may in many cases not affect the plasma unduly. The fourth diagnostic method discussed, optical emission spectroscopy, is non-perturbing; however, interpretation of spectral response is often difficult in low-pressure plasmas where the species are not in local thermodynamic equilibrium.

The field of plasma diagnostics is a large and varied one, and here we wish only to present the basics, applicable to the type of discharges used in the treatment of textiles, allowing readers to find more detailed and specific information relevant to their applications.

We recommend the following texts, which concentrate on or have included within, excellent sections on plasma diagnostics: Hutchinson (1994), Hippler

et al. (2000), Biederman (2004), Becker *et al.* (2005) and Ovsyannikov and Zhukov (2000).

2.2 Discharge electrical characteristics

The nature of the driving currents and voltages of a plasma discharge and their relationship can provide a lot of information about the bulk plasma properties, these being the physical and chemical plasma processes, the effective plasma impedance, the power absorbed in the plasma, the discharge efficiency and mode of operation. In general, the current–voltage relationship will be a complex function of the external parameters (e.g. geometry and method of plasma excitation), and will affect the intrinsic plasma parameters (e.g. potential, plasma density and temperature). This relationship is given essentially by the effective series impedance of the bulk plasma and the boundary sheaths that connect the plasma to the walls and electrodes. This impedance may be complex (i.e. have a reactive component) or, in some cases, may be mainly resistive. The latter is particularly relevant for d.c. plasmas. The type of measurements that can be made of the excitation voltage and current depends on the method of excitation of the plasma itself. For instance, measuring d.c. voltages and currents is a very different task from mid-frequency a.c. waveforms and those at RF frequencies. For discharges sustained by electrical means we believe all good diagnostic work on a plasma should start with determining the relationship between the discharge current and voltage.

2.2.1 Simple model of the d.c. plasma impedance

In plasmas produced by electrical means, the electrons (initially produced by cosmic radiation) are accelerated by the application of electric fields and transfer their energy to the neutrals by ionising collisions. This is a necessary process for sustaining the discharge. Ions and electrons lost by diffusion to the walls and recombination processes (three-body and radiative) must be replaced by electron impact ionisation of neutrals. The electrons, which have a much higher mobility than the ions, will absorb the largest amount of power from the driving electric fields and carry most of the discharge current.

For electrons in a weakly ionised plasma (dominated by electron–neutral collisions) the electrical conductivity is $\sigma = eN_{eo}\mu_e = e^2N_{eo}/M_e\nu_m$ (Lieberman and Lichtenberg, 1994). Here μ_e is the mobility, N_{eo} is the bulk electron density, M_e is the electron mass, e is the electronic charge and ν_m is the electron–neutral collision frequency. The conductivity then increases linearly with electron density and decreases with collision frequency; the latter is dependent on the density of the neutral particles (i.e. the neutral pres-

sure). Thus, we can see that the current density j ($= \sigma E$ where E is the electric field) in such a discharge is proportional to the plasma density N_{eo}.

For a typical weakly ionised argon plasma with $N_{eo} \sim 10^{16}\,m^{-3}$, electron temperature $T_e \approx 3\,eV$ (thermal speed $v_{th} \sim 10^6\,ms^{-1}$) and a pressure of $\approx 0.3\,Pa$ (mean-free-path $\lambda_{en} \approx 0.5\,m$), we have $\nu_m = v_{th}/\lambda_{en} \approx 2 \times 10^6\,s^{-1}$ and $\sigma \approx 78\,\Omega^{-1}\,m^{-1}$. This means, for a plasma column of cross-sectional area A of, for example, $2.5 \times 10^{-3}\,m^2$ and length L (cathode–anode separation) of 0.1 m, the bulk plasma resistance would be $R_p = L/A\sigma \approx 0.5\,\Omega$.

However, in the sheath regions at the cathode and anode, the electron concentration is small (negligible in most cases) and the d.c. sheath impedance, R_s, is much larger. We can approximate the sheath impedance to be $R_s \approx V_s/I_B \approx (V_p - V_c)/AeN_{io}C_B$ where A is the effective cathode area, $C_B = (eT_e/M_i)^{1/2}$ the ion acoustic (Bohm) speed, V_p the plasma potential M_i is the ion mass, and V_c the cathode potential. For $A \approx 3 \times 10^{-3}\,m^2$, $N_{io} \approx N_{eo}$ (quasi-neutrality approximation), $V_p - V_c \approx 100\,V$ and, given the plasma parameters stated above, this would give a sheath resistance of $R_s \approx 7.75\,k\Omega$. The sheath has greater impedance than the bulk plasma and in many low-pressure d.c. plasmas the sheath impendence will be about this value, i.e. a few kilo ohms.

2.2.2 The electrical characteristics of RF plasmas

In RF plasmas (typical excitation frequency of 13.56 MHz), the plasma conductivity σ_p can be introduced by linking the total current density to the electrodes, J_T, to the time-varying electric field, $\hat{E}$, by $J_T = (\sigma_p + i\omega\varepsilon_0)\hat{E}$ with $\sigma_p = (\varepsilon_0\omega_{pe}^2)/(i\omega + \nu_m)$. Here, σ_p is now complex, ε_0 is the permittivity of free space and $\omega_e = (N_{eo}e^2/\varepsilon_0 M_e)^{1/2}$ is the electron plasma frequency. Hence, we can consider the plasma to be either a dielectric or a conductor. For low frequencies ($\omega < \nu_m, \omega_e$) we find $\sigma_p \to \sigma_{dc}$. Here, the DC conductivity is, assuming a cold plasma, given by $\sigma_{dc} = \varepsilon_0\omega_{pe}^2/\nu_m = e^2N_{eo}/M_e\nu_m$. At high frequencies, the situation is complicated and it is often more useful to consider the dielectric constant, ε_p, rather than σ_p (for further details, see Lieberman and Lichtenberg, 1994).

2.2.3 I–V measurements on RF plasmas

Electrical characterisation of a plasma reactor is essential as a starting point for the successful interpretation of discharge processes within the chamber. Since the relationship between the nominal output of the generator and discharge conditions is unknown, a number of methods to infer the electrical characteristics of the plasma have been developed (Sobolewski, 1992; Hargis *et al.*, 1994; Braithwaite, 1997; Bakker *et al.*, 1999; Teuner *et al.*, 1999).

The RF current and voltage probe

Making discharge current and voltage measurements in RF systems is not as straightforward as in d.c. driven plasmas. Nevertheless, the measurements are very important, especially if they can be used to determine a change in the plasma process; for instance, the end point of an etching process, when a change in the chemical nature of a plasma causes a change in the effective impedance of the reactor and therefore a change in the driving electrical characteristics (Dewan *et al.*, 2001; Bose *et al.*, 1994).

Current and voltage sensors have been used on RF discharges in the Gaseous Electronics Conference (GEC) reference cell (Sobolewski, 1992; Hargis *et al.*, 1994) and other vessels (Braithwaite, 1997). They consist of an inductive loop and a cylindrical capacitor housed in a small metal unit inserted in the RF power line and are easily constructed from materials readily available in most laboratories. The probes provide real-time, non-intrusive electrical measurements, but require knowledge of the stray impedance in the power feed-through. An example is shown in Fig. 2.1. The capacitance C_s is that of two coaxial cylinders and the mutual inductance of the loop and power line, L_s, can be calculated from Ampere's law and Faraday's law. The sensor is positioned as close to the driven electrode as possible to minimise the effect of stray impedance. The outputs V_C and V_L are terminated at the 50 Ω input (R_{in}) of a digital oscilloscope, to minimise standing waves in the transmission line. The RF potential of the power line at the sensor, V_s, is calculated from the RC potential divider circuit, $V_s = [1 + (i\omega R_{in} C_s)^{-1}]V_c$. The voltage induced in the loop is related to the current, I_s, in the power line by Faraday's law, $V_L = -L_s(dI_s/dt)$, so that $I_s = -(V_L/\omega L_s)$. The current and voltage values at the RF-driven electrode (I_{el} and V_{el}) can be calculated by considering the parasitics in the power line between the I–V sensor and the driving electrode. An equivalent circuit model is shown in Fig. 2.2. The capacitances C_1 and C_2 are determined by the construction of the feed-through and electrode. The length of the current path to the

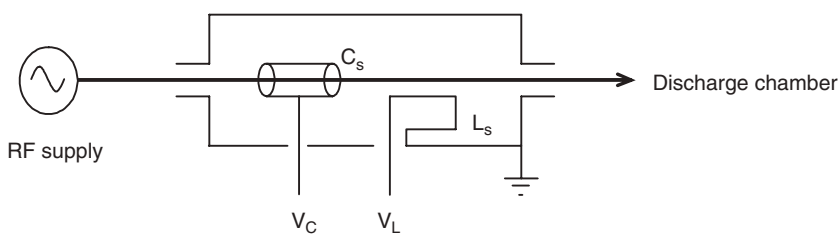

2.1 Schematic of a current–voltage sensor, consisting of a coaxial capacitor and an inductive loop. V_C and V_L are measured with respect to earth potential.

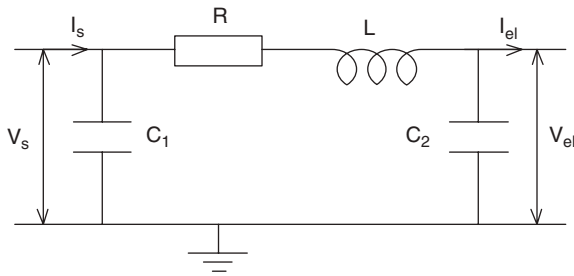

2.2 An equivalent circuit for the RF power line between the I–V sensor and the powered electrode (Hargis *et al.*, 1994; Braithwaite, 1997).

powered electrode and the return path create the inductance, L. The power line also has a small resistance, R.

The electrical characteristics of the discharge are found by calculating a transfer function for the values measured by the sensor (Hargis *et al.*, 1994). This can be represented by a transmission matrix of complex, frequency-dependent variables, which describe the equivalent LCR network in Fig. 2.2,

$$\begin{bmatrix} V_s \\ I_s \end{bmatrix} = \begin{bmatrix} a & b \\ c & d \end{bmatrix} \begin{bmatrix} V_{el} \\ I_{el} \end{bmatrix} \quad [2.1]$$

Assuming that the circuit is linear and reciprocal, the determinant of the transmission matrix is unity,

$$ad - bc = 1 \quad [2.2]$$

Consequently, Equation 2.1 rearranges to form,

$$\begin{bmatrix} V_{el} \\ I_{el} \end{bmatrix} = \begin{bmatrix} d & -b \\ -c & a \end{bmatrix} \begin{bmatrix} V_s \\ I_s \end{bmatrix} \quad [2.3]$$

The parameters a, b, c, and d can now be obtained from solving Equations 2.1 and 2.2 for open ($I_{el} = 0$) and closed ($V_{el} = 0$) circuit conditions to give,

$$a = \left(\frac{V_s}{V_{el}} \right)_{I_{el}=0} \quad c = \left(\frac{I_s}{V_{el}} \right)_{I_{el}=0} \quad \frac{b}{d} = \left(\frac{V_s}{I_{el}} \right)_{V_{el}=0} \quad [2.4]$$

This is done with the vacuum vessel vented, using a signal generator to provide an input waveform of a few volts amplitude. The powered electrode is securely earthed to create the closed-circuit condition and left electrically floating for open circuit. The voltage and current values at the RF-driven electrode can then be calculated from Equation 2.3. Using the peak values

of these parameters, the plasma impedance Z_{el} and rms power dissipated at the electrode P_{el} can be found, since, $Z_{el} = V_{el}/I_{el}$ and $P_{el} = (1/2)V_{el}I_{el}\cos(\phi)$. The angle ϕ is the phase difference between V_{el} and I_{el}. The phase angle between V_s and I_s can be measured directly from the oscilloscope. However, one must remember to compensate for the use of different length probes on the outputs of the sensor, since for RF the phase shift is appreciable, even in short transmission lines.

2.2.4 The current–voltage relationship in high pressure plasmas

In plasmas relevant to the processing of textiles, such as those struck at high pressure, it is important to observe the driving electrical characteristics of the source as an indication of its efficiency and mode of operation. In dielectric barrier discharges (DBD), filamentary and atmospheric-pressure glow discharge (APGD) modes can be distinguished through observation of the characteristic discharge current waveform. For instance, an APGD has only one current peak per half period, whereas a filamentary discharge has many narrow current peaks per half period. Monitoring of the discharge mode has important implications for materials processing. For example, Sira *et al.* (2005) compared the surface properties of polyethylene and polypropylene after surface modification in filamentary and APGD modes. The samples treated in APGD mode were more homogeneous and showed less roughness than those treated in the filamentary mode.

Borcia *et al.* (2005) measured the electrical characteristics of an atmospheric-pressure nitrogen DBD during surface treatment of test polymeric materials (UHMW polyethylene). Figure 2.3(*a*) shows the waveforms of the high voltage used to drive the discharge, and of the discharge current, with the polyethylene film placed on the aluminium cylinder. The power supply was found to generate mixed signals comprising high voltage pulses of variable width and repetition rate superimposed on a continuous sinusoidal waveform. The resulting high-voltage waveform ensured an optimum power level for driving the discharge, with peak-to-peak values in the 10–20 kV range, at a frequency of 80 kHz. Figure 2.3(*b*) shows an example of the Lissajous figures (charge-versus-voltage plot) obtained in the same experiment. These plots can be used to good effect when comparing the discharge process in air and nitrogen environments in terms of the discharge energy and the effect on the discharge parameters (polymer films or woven fabrics placed on the grounded electrode). For instance, the measurements of the electrical parameters in the case of nitrogen flowing through the discharge show values for the energy of the same order of magnitude as in air, that is in the 1–10 mJ range.

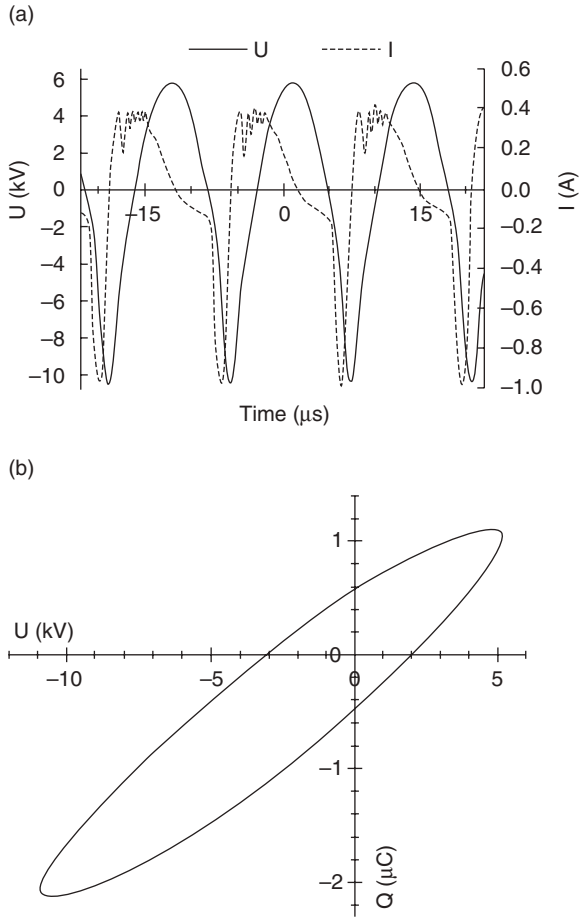

2.3 (a) High voltage and current waveforms of the DBD (1.8 mm gap, 80 litres min^{-1} N_2 flow rate). (b) Measured Lissajous figure (Q versus U plot) of the DBD (1.8 mm gap, 80 litres min^{-1} N_2 flow rate) (taken from Borcia *et al.*, 2005).

Lissajous figures have also been used by the same authors for DBD surface treatment of selected polymer films and fibres (Borcia *et al.*, 2003). From these, the energy surface density of the DBD (in $mJ\,cm^{-2}$) as a function of inter-electrode gap, and the nature of the sample placed on the grounded electrode was determined. Lissajous figures have also been used by Falkenstein and Coogan (1997) to determine the total transferred charge per cycle in a double-barrier discharge. Measurements of the behaviour of single micro-discharges between the metal and glass electrodes for both negative and positive polarities of the metal were made and a

theoretical Lissajous figure was constructed, which included stray capacitances, to compare against the experimental figures.

2.3 Electrical plasma diagnostics

Diagnostics based on the electrical properties of plasmas are perhaps the most frequently used methods of determining the local plasma parameters such as electron density, N_{eo}, temperature, T_e, and plasma potential, V_p. Of these, the Langmuir probe is probably the most important but its use is hampered by the complexity of probe theories. This is because there is no general theory that covers all the different types of plasmas. In this section, the theory of Langmuir probes and retarding field analysers is briefly given. For a more comprehensive treatment, the reader is referred to reviews by Demidov *et al.* (2002), Hershkowitz (1989), Chung *et al.* (1975), Swift and Schwar (1970), Schott (1968) and Chen (1965a).

2.3.1 Langmuir probes

Langmuir probes are cylindrical, spherical or planar conductors that disturb the local plasma by the formation of electrostatic sheaths. For large probes (probe radius $r_p >> \lambda_{De}$), these form when the (normalised) potential difference between the plasma and probe, $\eta_a = e(V_a - V_p)/k_B T_e$ with V_a the applied probe voltage, exceeds the Bohm potential, η_B (Riemann, 1991). For $\eta_a < \eta_B \approx -1/2$ (the exact value depends on the ion velocity distribution temperature, T_i) collisionless positive ions are accelerated from the surrounding plasma through a quasi-neutral presheath (roughly equal ion and electron densities) before reaching the Bohm speed where the sheath potential η (= $e(V - V_p)/k_B T_e$) = η_B. Here, the plasma quasi-neutrality breaks down and the rapidly increasing electric field reduces the electron density leaving a net positive space charge region called the sheath. For smaller probes, the position and potential of the boundary between sheath and presheath is not always clearly defined. The sheath thickness, which is a complicated function of η_a, probe geometry and plasma parameters, is usually expressed in units of Debye distance, $\lambda_{De} = (\varepsilon_o k_B T_e/N_{eo}e^2)^{1/2}$. By varying V_a and measuring the probe current, I_p, the probe I–V characteristic is obtained from which the local plasma parameters can be derived.

Since probes are necessarily small, to minimise current drain and plasma disturbance, planar probe sheaths can be hemispherical due to edge effects (Ingram *et al.*, 1990). This causes the ion current to continually increase with η_a (<0) due to the expanding non-planar sheath. Guard rings placed around the planar probe can significantly reduce the sheath curvature (Booth *et al.*, 2000), resulting in ion current saturation (i.e. ion current independent of η_a), allowing the simpler planar probe theory to be used. Only spherical and cylindrical probes, which are considerably more complicated, will be considered here.

Elementary Langmuir probe theory

In Fig 2.4 a probe I–V characteristic is shown divided into three regions referred to as the orbital motion limited (OML, $\eta_a > 0$), electron retardation ($\eta_f < \eta_a < 0$) and ion current regions ($\eta_a < \eta_f$). The point of zero current is the probe's floating potential, η_f, which is the potential acquired by an electrically isolated object placed in the plasma. At plasma potential ($\eta_a = 0$), a probe of area A_p collects the random thermal electron current given by $I_{eo} = (1/4)eA_pN_{eo}(8k_BT_e/\pi M_e)^{1/2}$. Since in low-temperature plasmas T_e ($\approx$ 3 eV) >> T_i ($\approx$ 0.03 eV) and $M_i >> M_e$ the ion current is negligible and this equation can be used to obtain the electron density, provided T_e and V_p are known. The plasma potential is usually indicated by the presence of a kink or knee but often this can be difficult to identify and the more accurate derivative method can be used. Here, a maximum in dI_p/dV_a or a zero crossing in d^2I_p/dV_a^2 indicates V_p. Other methods define V_p to be the intersection of extrapolations from the electron retardation and OML regions or the point of deviation from linearity. The latter method is strictly applicable only for Maxwellian electrons. These methods are compared in Fig. 2.5 where it is seen that the inferior extrapolation method overestimates V_p (= 25.2 V) by 0.7 V. The derivatives can be obtained electronically by differentiator circuits (Godyak *et al.*, 1992) or by using the beat method (Amemiya,

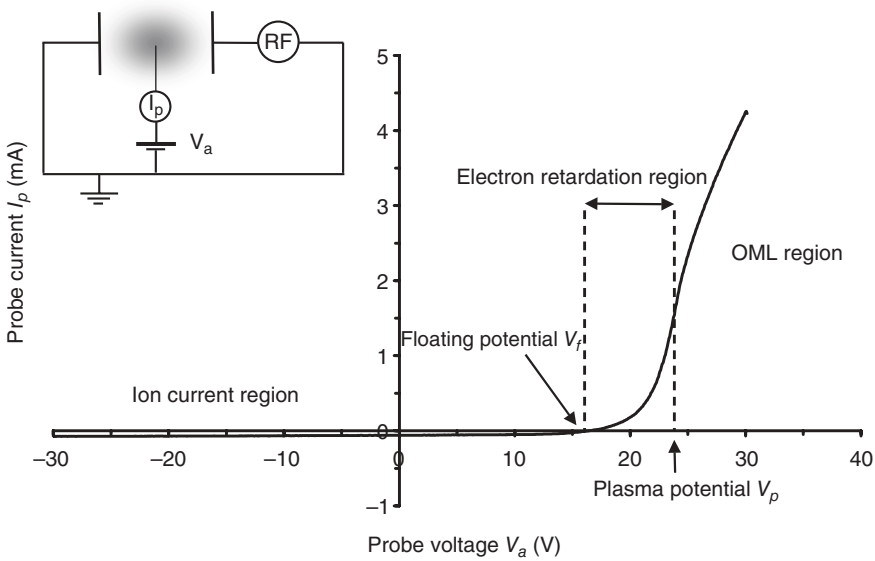

2.4 Typical actively compensated Langmuir probe I–V characteristic taken from an argon capacitively coupled RF plasma at low pressure. Analysis of the characteristic is divided into the OML, electron retardation and ion current regions. Insert: Schematic of the discharge circuit including the Langmuir probe.

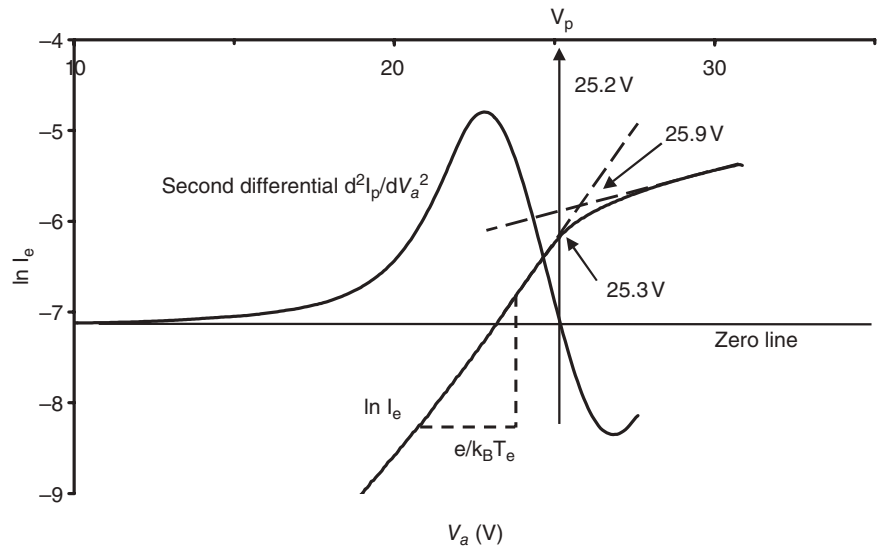

2.5 Second derivative d^2I_p/dV_a^2 of Fig 2.4 superimposed on a $\ln I_e$–V_a plot. Plasma potential is indicated by the zero-crossing of d^2I_p/dV_a^2 and the deviation from linearity in a $\ln I_e$–V_a plot. In this plot T_e can be also be obtained from the gradient.

1986). They can also be obtained numerically using, for example, Savitzky–Golay filters (Fujita and Yamazaki 1990), finite impulse response filters (Kimura *et al.*, 1991), or Hayden filters (Palop *et al.*, 1995).

In the OML region ($\eta_a > 0$), the ions are rapidly repelled and the electrons are accelerated and collected by the probe. Due to their temperature, the electrons acquire angular momentum in the probe's radial electric field and their trajectories become curved. Some trajectories intersect the probe's surface while others curve around and miss the probe. For electrons that have a Maxwellian velocity distribution far from the probe and for which $\lambda_{en} >> \lambda_{De} >> r_p$ (with the electron-neutral mean free path and r_p the probe radius) this situation is well approximated by the orbital motion limited theory (OML). The electron current is then given by

$$I_e = A_p e N_{eo} \left(\frac{k_B T_e}{2\pi M_e} \right)^{1/2} \left(\frac{2}{\sqrt{\pi}} \right)^{2-s} \qquad [2.5]$$

where $s = 1$ for cylinders and $s = 2$ for spheres. Due to simplifying approximations, this expression is only valid in the cylindrical case, for $|\eta_a| > 2$. A review of OML theory, which is a special case of the more general orbital motion theory (OM) of Laframboise (see Kennedy and Allen, 2003), can be found in Allen (1992a). From this equation, a plot of I_e against $V_a^{s/2}$ gives a straight line from which N_{eo} can be obtained from the gradient. Typically,

the electron density obtained by this method is within 10% of the density obtained at V_p (Hopkins and Graham, 1986).

For $\eta_f < \eta_a < 0$, the electrons are gradually repelled and for Maxwellian electrons the current may be written as $I_e = I_{eo}\exp(\eta)$. By subtracting the ion current from the I–V curve and plotting ln I_e against V_a, a straight line of gradient e/k_BT_e is obtained (see Fig 2.5). The temperature is most accurate near to the plasma potential but deviations from linearity caused by, for example, a non-Maxwellian electron distribution, incomplete RF compensation (see section Radio frequency (RF) plasmas) or probe contamination, can result in appreciable errors. Alternatively, T_e can be obtained from the relation $I_e/(dI_e/dV_a) = k_BT_e/e$ (Chen, 2001). Since in most plasmas the electrons are non-Maxwellian (e.g. Godyak *et al.*, 1992), use of these (or other) methods yields the effective or characteristic temperature, T_e. The remarkably linear line, indicating 'Maxwellian' electrons, in the ln I_e–V_a plot (Fig 2.5) is known as Langmuir's paradox. A common method of ion current subtraction is by linear extrapolation from the ion current region ($\eta_a < \eta_f$). However, a better method is to subtract a theoretical fit to the experimental ion current using the appropriate theory of ion collection (see later).

The second derivative of the probe's I_e–V_a characteristic can be used to obtain the electron energy distribution function (EEDF) (Godyak *et al.*, 1992). This is known as the Druyvesteyn method and is applicable to any non-concave probe in an isotropic plasma with collisionless electrons. The EEDF, f(E), can be obtained from:

$$f(E)|_{E=e(V_p-V_a)} = -\frac{4}{A_p e^2}\left(\frac{M_e(V_p - V_a)}{2e}\right)^{1/2}\frac{d^2I_e}{dV_a^2} \qquad [2.6]$$

Numerical integration of this function yields the electron density and the effective temperature can be obtained from $<E> = 3eT_e/2$ where $<E> = M_e <v^2>/2$ is the average electron energy. Note that this method is insensitive for electron energies greater than $e(V_p - V_f)$.

In the ion current region ($\eta_a < \eta_f$), the probe current is dominated by the accelerated positive ions. For collisionless conditions, in which the ion-neutral mean free path $\lambda_{in} >> \lambda_{De}$, the ion current can be approximated by the OML theory (Equation 2.5 with subscript e substituted for i). This theory is only applicable to small cylindrical ($r_p/\lambda_{De} \leq 3$ for $\eta_a \leq -10$) or spherical probes ($r_p << \lambda_{De}$). For larger probes parametric expressions approximating the numerical results of Laframboise (Chen, 2001) can be used. In another approach, Allen *et al.* (1957, ABR) (for spheres) and later Chen (1965b) (for cylinders) developed a collisionless theory in which cold ions ($T_i = 0$) are accelerated radially along the electric field lines. By fitting the theoretical ion current to the measured one, the electron density, as fitting parameter, can be obtained. Many studies have shown disagreement

between the OM and ABR theories (Hopkins and Graham, 1986; Sudit and Woods, 1994; Chen, 2001) with the ABR theory giving better agreement with the knee density usually to within a factor of 2 (Passoth *et al.*, 1997; Bryant *et al.*, 2001a). This has been attributed to ion-neutral collisions destroying orbital motion and promoting radial motion, increasing the ion current to the probe (Stangeby and Allen, 1971). A criterion for the applicability of orbital motion theories with finite λ_{in} has been suggested by Chen (1965b), Shih and Levi (1971) and Annaratone *et al.* (1992). For weakly to moderately collisional sheaths ($\lambda_{in} \sim \lambda_{De}$) other theories have been developed in which collisions have been incorporated into spherical ABR theory (Self and Shih, 1968), modeled as a perturbation (Shih and Levi, 1971) resulting in a correction factor, or considered at a kinetic level (Chou *et al.*, 1966; Tichý *et al.*, 1994). At higher pressures, the sheath is fully collisional ($\lambda_{in} << \lambda_{De}$) and ion motion is governed by diffusion and mobility (Su and Lam, 1963; Cohen, 1963 for spheres; Kamitsuma and Teii, 1982 for cylinders).

Radio frequency (RF) plasmas

In RF plasmas, the plasma potential oscillates, resulting in a time-dependent voltage drop across the sheath. This distorts the I–V characteristic, increasing the time-averaged electron current in the retardation region and shifting the characteristic towards the negative voltages, so that conventional probe theory cannot be used (Boschi and Magistrelli, 1963). In general, there are two methods for removing the RF voltage and associated harmonics across the probe sheath: (i) use of a passive probe in which a series of LC resonant filters (Chatterton *et al.*, 1991) or low-pass filters (Annaratone and Braithwaite, 1991) are placed in the probe circuit to force the probe to follow the instantaneous plasma fluctuations; or (ii) use of an active probe in which phase and amplitude matched RF voltage waveforms are applied to the probe tip (Dyson *et al.*, 2000). This technique has the advantage of providing local information of the phase and magnitude of the plasma harmonics. Once the probe is compensated, conventional Langmuir probe theory can then be used to extract the plasma parameters.

Electronegative plasmas

Obtaining the negative ion density, N_{no}, and temperature, T_n, directly from the measured I–V curve is made difficult because $T_e >> T_n \sim 0.1$ eV so that the negative ion current is negligible in both the retardation and OML regions. For collisionless sheaths and critical ratios $\alpha_c = N_{no}/N_{eo} \approx 2$ or less, the presheath is dominated by electrons and positive ions (electropositive) and the presence of negative ions cannot be detected by the probe. For ratios greater than $\alpha_c \approx 2$ and $\gamma_c = T_e/T_n \approx 10$ (Braithwaite and Allen, 1988),

the Bohm potential is reduced to approximately $\eta_B \approx -1/2\gamma$ and the presheath is populated by electrons, positive and negative ions (electronegative). In the presence of ion-neutral collisions, α_c increases with pressure but γ_c remains constant (Bryant, 2003). For $\alpha_c < \alpha < \alpha_M$, sheath instabilities can form (Kono, 2003), which invalidates the use of the probe. The instabilities are not present for $\alpha > \alpha_M$ and the positive ion current, which is proportional to $\alpha\gamma^{-1/2}$ (Bryant *et al.*, 2001b), can then be used for diagnostics. For an ideal planar probe (no edge effects), the ratio of electron to ion saturation currents (current ratio method) can then be used to give α provided γ is known (Amemiya, 1990). Chabert *et al.* (1999) used a combination of planar and cylindrical Langmuir probes to determine the negative ion density by this method in an SF_6 helicon reactor. By extending the ABR theory to include negative ions, Amemiya *et al.* (1999) suggested fitting the theoretical ion current characteristic to an experimental curve to determine α (if γ and N_{eo} are known). The method was applied experimentally, after correcting for ion-neutral collisions, by Bryant *et al.* (2001b) in a pure RF oxygen plasma. Negative ions, when present in sufficient quantities, can cause T_e to increase due to electron losses by attachment and depress the low-energy part of the EEDF, revealing the negative ion EDF. Under these conditions, a modified Druyvesteyn method can be used to measure both α and γ simultaneously (Amemiya and Yasuda, 1997).

Magnetised plasmas

In magnetic fields, charged particles gyrate around magnetic field lines at the Larmor radius $r_{Li,e} = M_{i,e}\, v_\perp/qB$, where $v_\perp$ is the angular velocity and B the magnetic field. Motion parallel to field lines is unaffected but motion across field lines is impeded due to gyration. This causes anisotropy in the particle's velocity distribution (Aikawa, 1976), introducing additional complexity into probe theory and analysis. In weakly collisional conditions, the effective mean free path $\lambda_{in,en}$ across the magnetic field is of the order of the Larmor radius, making the problem collisional even when $r_{Li,e} < r_p$ and $\lambda_{in,en} >> r_p$. Generally, probe operation can be characterised by the parameters $\max(\lambda_{De}, r_p)/r_{Li,e}$ and B/pressure (Chung *et al.*, 1975). At high pressures, $\lambda_{in,en} < r_{Li,e}$ and the action of the B-field is reduced by collisions (Niyogi and Cohen, 1973). For weak B-fields, $\max(\lambda_{De}, r_p)/r_{Li,e} << 1$ and particle motion are unaffected by the B-field and zero-magnetic field probe theory can be used. For moderate B-fields, $\max(\lambda_{De}, r_p)/r_{Le} \sim 1$ (with $\max(\lambda_{De}, r_p)/r_{Li} << 1$) and electron gyration can no longer be neglected. The preferential motion of electrons along the field lines causes the electron current at plasma potential and in the retardation region to be reduced, resulting in rounding of the knee. As η_a (<0) is increased, the probe characteristic becomes less distorted as the higher energy electrons have larger Larmor radii (Sanmartin, 1970; Sonmor and Laframboise, 1991). Use of standard probe analysis in

this region causes T_e to be overestimated and V_p underestimated. For cylindrical and planar probes, the reduction is minimal when the probe's axis is perpendicular to the field lines (Rubinstein and Laframboise, 1983; Thompson and Bradley, 2001). The EEDF can be inferred, for cylindrical symmetry about the *B*-field vector, by employing a rotational planar probe (Klagge and Lunk, 1991; Mezentsev *et al.*, 1988). In the ion current region the motion of unmagnetised ions can be described as for the zero-magnetic field case (Passoth *et al.*, 1997).

2.3.2 The retarding field analyser (RFA)

The RFA can be immersed in the plasma bulk as a gridded probe or mounted on one of the electrodes (or substrate) and consists of a series of grids and a collector plate (see Fig 2.6). Gridded probes can be used to measure the anisotropy of T_e and the EEDF. To avoid drawing excessive electron currents and perturbing the plasma, the first grid, g1, is usually biased at a potential $V_{g1} < V_p$ (Ingram *et al.*, 1990). Mounted RFAs, which are usually used to measure the ion energy distribution function (IEDF) at electrodes, have g1 biased at the electrode potential to avoid perturbing the adjacent sheath. Generally, two modes of operation, filter and normal mode,

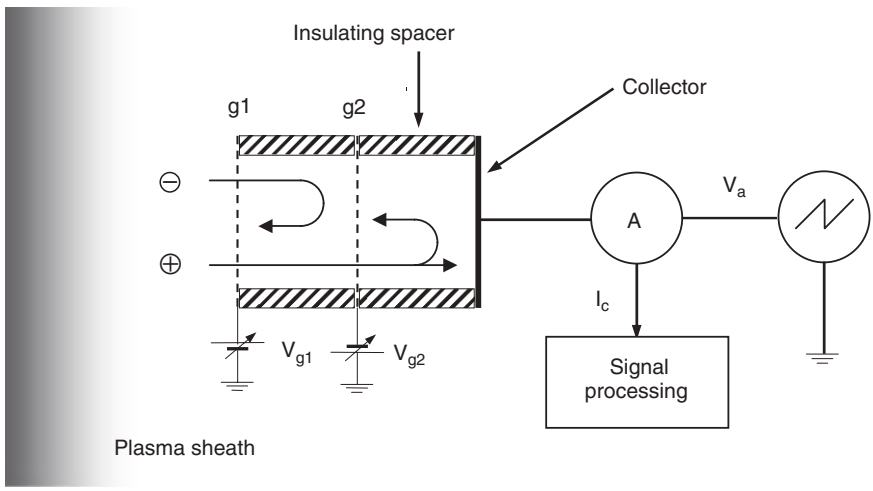

2.6 Schematic of a RFA and external circuit. The first grid, g1, is biased at the electrode potential (mounted RFA) or biased slightly below plasma potential (gridded probe). In normal mode, plasma electrons are repelled by g2 while the positive ions are accelerated through g2 and are then selectively repelled, according to their energy, by a ramping retardation potential applied to the collector.

are possible with the remaining grids and collector. Ingram *et al.* (1990) concluded that filter mode exhibited more disadvantages than normal mode. In this mode, the second grid, g2, is used to repel the unwanted plasma species and a linear voltage ramp, V_a, is applied to the collector to filter the remaining species. In gridded probes $V_{g2} > V_p$ (by several volts) to repel the positive ions whereas in mounted RFAs V_{g2} can be negative ($<-10T_e$) to reject the electrons or positive (> maximum ion energy) to sample the high energy part of the EEDF (Ingram and Braithwaite, 1988). For RFAs with g1 grounded, the maximum ion energy can be used to measure V_p (Ingram and Braithwaite, 1988) and T_e (Sowa *et al.*, 2002) if the plasma sheath is suffiently collisionless.

In general, for an ideal planar RFA of area A, the particle velocity distribution function (VDF) as sampled at g1, $f_1(v_1)$, can be obtained from the first derivative of the I–V characteristic (see Ingram and Braithwaite, 1988) by

$$\frac{\mathrm{d}I_c}{\mathrm{d}V_c} = -T_t A \sum_{i=1}^{N} \frac{q_i^2 f_1^i(v_1)}{M_i} \qquad [2.7]$$

with $V_c = V_a - V_{g1}$; q_i the charge for the ith species; and $T_t = T_1 T_2$, the total grid transmission. Note that, for mounted RFAs, the observed VDF, $f_1^o(v_1)$, is a weighted sum over N ionic species. Since a plot of $\mathrm{d}I_c/\mathrm{d}V_c$ against V_c is a plot of $(-T_t A q^2/M) f_1^o(v_1)$ against $(M/2e)v_1^2$, the EDF can be obtained by plotting $(\mathrm{d}I/\mathrm{d}V_c)/V_c^{1/2}$ against V_c (Allen, 1992b). Alternatively, the velocity distribution may be obtained by plotting $\mathrm{d}I/\mathrm{d}V_c$ against $V_c^{1/2}$, thereby avoiding the singularity at $V_c = 0$. For gridded probes, the EDF must be shifted by an amount $V_p - V_{g1}$ to obtain the EEDF.

In designing an RFA, the grid apertures of g1 should be of the order of, or less than, λ_{De} to prevent plasma penetrating through the grid and to minimise distortion of the sheath's electric field (Edelberg *et al.*, 1999a). To prevent ion–neutral collisions in the RFA from causing spurious signals, the overall thickness should be less than λ_{in}. This can be accomplished by differential pumping (Flender and Wiesemann, 1994) or by design (Ingram and Braithwaite, 1988, Sowa *et al.*, 2002). The collector is usually tantalum or tungsten to reduce secondary electron emission (by ion bombardment), which can be reduced further by inserting additional grids (Böhm and Perrin, 1993; Kortshagen and Zethoff, 1995). The energy resolution of the RFA is limited by defocusing of ions or electrons in the vicinity of the grid apertures (Simpson, 1961) and by space charge effects (Donoso and Martin, 1990; Honzawa *et al.*, 1993). In particular, defocusing is caused by distortion of the field lines leading to a reduction in the translational velocity component and distorting the EDF (Edelberg *et al.*, 1999a). A number of studies have shown the resolution to be a complicated function of grid separation,

wire diameter and aperture radius (Sakai and Katsumata, 1985; Donoso and Martin, 1986) and that it can be improved by using additional grids (Enloe and Shell, 1992). Other possible sources of error that may distort the EDF are due to the particle collection by grid apertures (Moskalev, 1970) and the finite size of the analyser (DeNeef and Theiss, 1979).

Other RFA designs can measure the ion angle distribution at grounded (Liu *et al.*, 1990) or driven (Woodworth *et al.*, 2002) electrodes: IEDFs at driven electrodes (Edelberg *et al.*, 1999b), and three-dimensional EDFs in the bulk plasma by rotating a conventional gridded probe (Iwama *et al.*, 1988) or by using a directional analyser (Stenzel *et al.*, 1983). Finally, the RFA can be combined with a quadrupole mass spectrometer to obtain mass and energy resolved IEDFs (Thompson *et al.*, 1986).

2.3.3 Other probe techniques

With reference to Fig. 2.4 (insert), the Langmuir probe forms part of the external discharge circuit with the restriction that $A_p/A_{gnd} << (2\pi M_e/M_i)^{1/2}$ (Ingram *et al.*, 1990), with A_{gnd} being the total grounded area, to minimise perturbation of the plasma. In electrodeless discharges, such as inductively coupled plasmas, there is insufficient grounded surface area so that the Langmuir probe invariably perturbs the plasma. By using floating probe techniques such as double (Welzel *et al.*, 2004), direct-display triple (Alami *et al.*, 2005, Kamitsuma *et al.,* 1977), emissive (Bradley *et al.*, 2004) or, more recently, hairpin resonator probes (Piejak *et al.*, 2005) this can be avoided. These probes have the additional advantage of following the instantaneous plasma fluctuations and are ideal for time-resolved plasma diagnostics.

2.4 Plasma mass spectrometry

Plasma mass spectrometry is a well-developed technique that provides information on the identity of the neutral and charged species present in a discharge, and their relative fluxes to a material surface or substrate. The technique is also an ideal tool for understanding the behaviour of plasmas with complicated mixtures of chemical precursors. There are many excellent and detailed reviews of this technique as applied to plasma discharges; for instance, Zeuner (2004) and Jarvis *et al.* (1990). We only discuss the fundamentals here, highlighting how mass spectrometry is used in the areas of residual gas, neutral and ion plasma analysis.

2.4.1 Commercial mass–energy spectrometers

A typical mass–energy spectrometer is shown in Fig. 2.7. This example is the Hiden electrostatic quadrupole plasma (EQP) 300 mass spectrometer

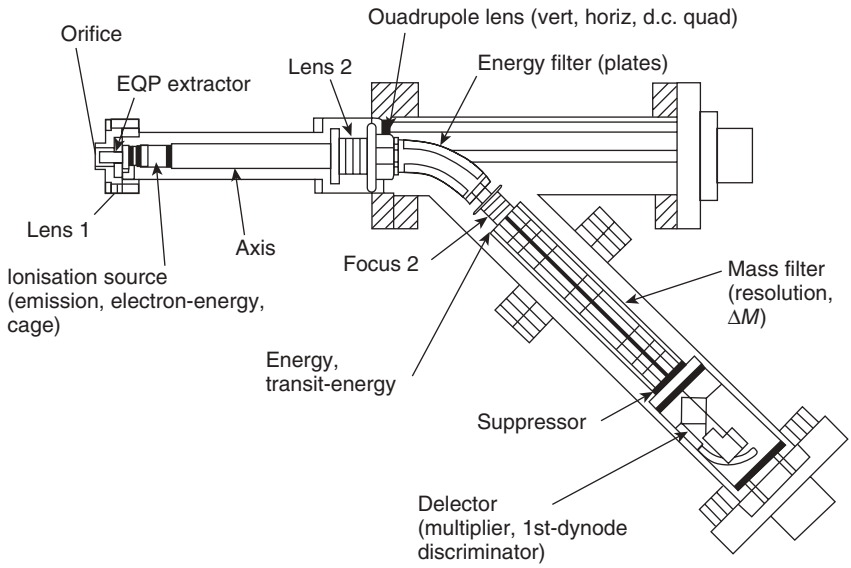

2.7 Schematic of the Hiden Analytical EQP300 mass spectrometer apparatus (Hiden).

(Hiden Analytical Ltd). Other examples include the Balzers PPM421 plasma monitor as used by Kusano *et al.* The EQP is capable of resolving particles of mass up to 300 AMU and can measure the energies of positive and negative ions over a range of ±1000 eV with respect to ground. Sampling is done through an orifice, typically 10 to 500 microns in diameter, which is in contact with the plasma via the plasma sheath. This is a region of space-charge that exists between the bulk plasma and a surface, which is at a different potential to the plasma (Lieberman and Lichtenberg, 1994). To minimise distortion of the sheath electric field, the orifice diameter must be less than the Debye length. However, in the absence of an electric field downstream from the plasma the sheath electric field can penetrate through the orifice (Liu *et al.*, 1990). This causes low energy ions to be defocused into the orifice walls or lost in the field-free region. In the Hiden system the first lens, the extractor, is typically biased (negatively) up to several tens of volts relative to the orifice potential. The electric field then reduces field penetration and focuses the ions into the remaining lenses. Computer control is used to set voltages on the lenses and electrodes inside the instrument, which number around twenty. Groups of these lenses focus the ion beam at each of the mass and energy analysis stages. The latter is achieved with a 45° electrostatic cylinder sector arrangement (Hiden). Other energy selection methods, including cylindrical mirror analysers, are discussed in more detail by Zeuner (2004). Once past the analysis stages, the ion beam

is converted into an electrical signal by either a Faraday cup or a high gain channeltron (continuous dynode) multiplier.

Neutral species entering the spectrometer are ionised, before the analysis stages, by an electron impact ion source (e.g. see Brink, 1966), situated close to sampling orifice. The ionised particles are extracted from the source by a system of electrically biased lenses. Typical electron energies of 70 eV in the source can cause molecules, particularly large organic molecules, to split into smaller ionised fragments. The additional peaks appear in the mass spectra as fragmentation patterns whose parent molecules can be identified by comparison to a database. When no fill gas is present in the plasma chamber, the ion source can be used for troubleshooting and calibration of the mass and energy analysis stages. To analyse only plasmaion species, the ion source is switched off.

The mass spectrometer housing is pumped to pressures below 10^{-4} Pa to avoid damage to the channeltron detector and ion source filaments. The low-pressure environment also ensures that there are insignificant collisions of ionised species (e.g. scattering, molecular dissociation, reactions involving radicals, etc.) en route to the detector. Additionally, the small orifice allows plasmas of pressures up to about 200 Pa to be sampled. At higher pressures, a two- or three-stage pressure reduction system is necessary (e.g. Singh *et al.*, 1999).

2.4.2 The quadrupole mass filter

The mass filter commonly used in many plasma research laboratories is the quadrupole (Dawson, 1976). As the name suggests, four parallel rods form the active part of the mass filter (see Fig. 2.8). Ideally, the rod's cross-section should be hyperbolic but, in practice, cylindrical geometry is used, since this is easier to manufacture and the loss in resolution is acceptable. By applying d.c. and RF voltages (V_{DC} and V_{RF}) to the rods, the time-varying electric fields will cause the ions to oscillate as they traverse the filter, resulting in a mass filtering action. Ions with the critical mass to charge (M/q) ratio will

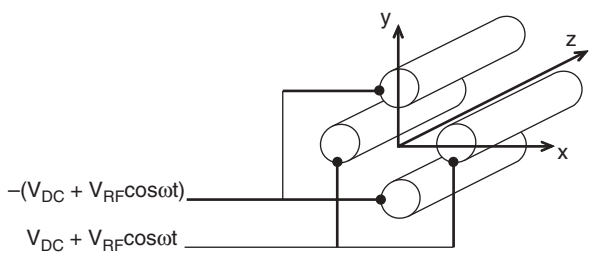

2.8 Schematic of a quadrupole mass filter. Ions pass through in the z-direction.

have stable trajectories and pass through the filter. For others, the oscillation amplitude increases until they are absorbed by the walls or rods (McDowell, 1963; White and Wood, 1986). The critical M/q ratio depends only on the ratio $k = V_{DC}/V_{RF}$, so that a mass spectrum is obtained by scanning through the M/q values on a scan line (with $V_{DC} = kV_{RF}$) for each value of k. The mass resolution is given by $\Delta M = k_1 E/f^2 L^2$ with k_1 a constant, f the RF frequency, L the quadrupole length and E the ion entrance energy. Higher resolution can be achieved by using longer electrodes but their uniformity and positioning are critical to the accuracy of the instrument. Also, the transmission decreases with increasing resolution. In practice, the position of entry, the ion's radial velocity component and the presence of fringing electric fields also affect the filtering action. The incident ion beam is then restricted at the analyser's entrance by a circular aperture. Fringing fields are minimised by use of additional filters positioned in-front or behind the quadrupole.

2.4.3 Residual gas analysis (RGA)

In RGA analysis, the spectrometer is used to sample the neutral species from an evacuated plasma chamber. The mass spectrum represents the residual gas (i.e. impurities) that originates from vacuum seal leaks and out-gassing from the chamber walls and spectrometer housing. For some plasma processes the presence of these impurities is detrimental, so this information can be invaluable. RGA analysis can also be used to trace sources of leaks. This is usually done by squirting, for instance, helium around vacuum seals outside the chamber with leaks detected by the spectrometer as sudden increases in the helium counts. The partial pressure of gas, effusing through the orifice, at the ion source is given by $P_L = P_{ch}\,[R^2/(R^2 + L)]$ with R the orifice radius, L the distance from the orifice and P_{ch} the plasma chamber pressure (Coburn and Kay, 1971). To ensure that the partial pressure of residual gas from the spectrometer housing, P_{sh}, is negligible during RGA analysis, we require $P_L >> P_{sh}$.

2.4.4 Neutral plasma analysis

By applying a large positive potential (> the plasma potential V_p) to the extractor (Hiden), the positive plasma ions are repelled, allowing the neutral plasma species to be analysed. This technique is used, for example, to monitor changes in gas composition, identify plasma fragmentation products and differentiate between neutrals that have originated from the walls and from the processed work piece, and those formed in the plasma itself. In some environments, the neutral plasma spectrum plasma can be complex in nature, consisting of many tens if not hundreds of different masses, with

the equilibrium concentrations a sensitive function of the discharge parameters (e.g. see Haddow *et al.*, 2000). As an example, Fig. 2.9 shows the neutral mass spectra taken in a continuous wave 13.56 MHz plasma polymerising discharge run in acrylic acid (Barton *et al.*, 2003).

Threshold ionisation mass spectrometry

Through variation of the electron energy in the ion source, near the ionisation potential of the species under study, it is possible to identify radical species in the plasma. This technique has been used to good effect in the identification of radicals such a CF_3 and CF_2 in CF_4 RF plasmas (Schwarzenbach *et al.*, 1997). Any detected ionised species could have come from dissociative ionisation of a molecule when the electron impact energy exceeds its ionisation potential. Since dissociative ionisation requires more energy to be transferred by the electron, the energy for this is higher than the ionisation of the radical by approximately the binding energy. With a good electron energy resolution in the ion source, it is possible to differentiate between ions produced from radicals and from dissociation. This technique is best used by comparing signals generated when the plasma is off (only process gas) and when it is on (gas plus ionisation of radicals). As identified in Biederman (2004), this technique has been used to detect SiH_x radicals (Kae-Nune *et al.*, 1995; Robertson and Gallagher, 1986), CF_x radicals (Pecher and Jacob, 1998) and CH_x radicals (Singh *et al.*, 1999).

Electron attachment mass spectrometry

In this technique, negative ions are created in the ion source from electron attachment onto electronegative species such as fluorine, oxygen and

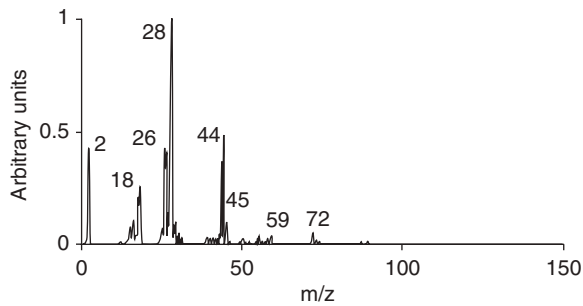

2.9 Electron impact (neutral species) mass spectrum of 5 W plasma, without applied RF substrate bias. m/z: 26 = $C_2H_2^+$; 28 = $C_2H_4^+$, 28 = OC^+, 28 = N_2^+; 44 = $C_2OH_4^+$, 44 = CO_2^+; 72 = $C_3H_4O_2^+$. There is a detectable signal in the neutral monomer at mass 72; however, the largest signals come from fragments of this molecule (taken from Barton *et al.*, 2003).

chlorine containing process gases, through dissociative attachment $AB + e^- \rightarrow A^- + B$ (Stoffels *et al.*, 1998; Rees *et al.*, 1998). The electron energy is set low, between 0 and 10 eV, in order to coincide with the resonance cross-section. Also, very limited fragmentation of the parent negative ion occurs, so a given molecule yields only a few different negative ions. This facilitates identification of components in a gas mixture. It is particularly advantageous for detection of large, fragile molecules, which break up after ionisation, but can be easily transformed into large negative ions.

2.4.5 Positive ion analysis

By turning off the ion source and using the energy filter in combination with the quadrupole, the instrument can sample plasma ions directly. The ions, after traversing the sheath adjacent to the orifice, arrive with a distribution of energies. The detected ion energy represents the potential at which the ions underwent their last collision process. These processes include in-elastic interactions such as ionisation, resonant (i.e. $A^+_{fast} + A_{slow} \rightarrow A_{fast} + A^+_{slow}$) and non-resonant (i.e. $A^+_{fast} + B_{slow} \rightarrow A_{fast} + B^+_{slow}$) charge transfer and elastic interactions such as polarisation scattering. Fast neutrals generated by charge transfer collisions have been observed by Janes and Börnig (1993). In low pressure d.c. plasmas, the ion energy distribution function (IEDF) has a single peak near to the plasma potential where most of the ionisation takes place. For collisionless sheaths, the peak width (full width at half maximum) is proportional to the electron temperature and the plasma potential is determined by the maximum ion energy. As the sheath becomes collisional, a tail then extends to the lower energies (Lieberman and Lichtenberg, 1994). However, in RF excited plasmas (e.g. those excited at 13.56 MHz), the sheath potential drop and its width vary approximately sinusoidally (usually higher harmonics are present) at the driving frequency. In some situations this manifests itself in the IEDF being shifted to higher energies (Riemann, 1989), becoming also wider and often accompanied with peak splitting (see review by Kawamura *et al.*, 1999). The modification of the IEDF by RF bias was used by Barton *et al.* (2000) to change the ion flux of argon ions bombarding a polymeric surface.

By selecting ion energies corresponding to the IEDF peak (near to V_p), the bulk plasma positive ion mass spectrum can be measured. Figure 2.10 shows the ion mass spectra in the same polymerising discharge as shown in Fig. 2.9. The spectrum reveals the complex nature of the positive ion species in the discharge. Plasma ion mass spectrometry has also been used in a pulsed glow discharge operated in CH_4–argon mixtures, for the treatment of PVDF in textile modification applications (Vohrer *et al.*, 1998), to observe the long-term time dependence of H_2F^+. As polymerisation takes place when the plasma is turned off, a film covers the substrate and the usually ablated H_2F^+ signal in the mass spectrum is subsequently reduced.

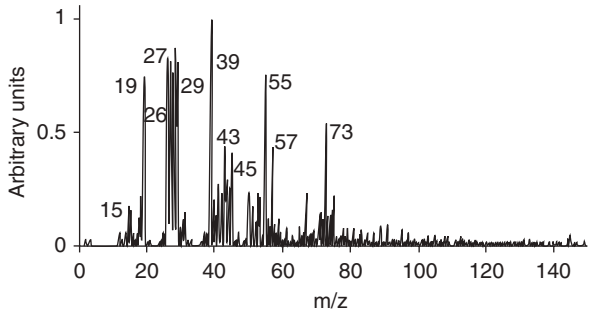

2.10 The positive ion mass scan at 5 W without applied RF bias. We assign the masses to the following; 15 = CH_3^+; 19 = OH_3^+; 26 = $C_2H_2^+$; 27 = $C_2H_3^+$; 29 = $C_2H_5^+$, COH^+; 43 = $C_2OH_3^+$; 45 = $C_2OH_5^+$; 59 = $C_3OH_7^+$; 73 = $C_3O_2H_5^+$. (taken from Barton *et al.,* 2000).

2.4.6 Negative ion analysis

Due to their low temperature (≈ 0.1 eV), negative ions created in the plasma bulk are usually confined to the discharge region by the boundary sheaths. However, in sufficient quantities their presence can affect the sheaths, leading to a reduction of the positive ion fluxes to the electrode and spectrometer (Lieberman and Lichtenberg, 1994). There are a number of techniques of extracting the bulk plasma negative ions. One such technique involves modulating the applied power (e.g. RF excitation) in such a way as to depress the local plasma potential below that of the extractor electrode (Howling *et al.*, 1993a). In an RF plasma, a positively biased orifice is used to attract the negative ions (Sasaki *et al.*, 1997). In other methods, the plasma potential is modulated with the electrode kept at a fixed bias, e.g. in pulsed (10 Hz–10 kHz) square wave RF silane discharges (Howling *et al.*, 1993b), and in other similar plasmas, e.g. by Overzet *et al.* (1989). In some plasmas, for example in reactive magnetron sputtering of metals in O_2 atmospheres, the negative ions (O^- and O_2^-) have enough intrinsic energy to overcome the small negative repelling potential of the plasma sheath at the orifice to be detected directly (Mišina *et al.*, 2003; Zeuner *et al.*, 1998). In an asymmetric capacitively coupled RF plasma, Zeuner *et al.* (1996) observed negative ions, at the grounded electrode, of energies comparable to the d.c. bias on the driven electrode. They concluded that the negative ions were formed in the vicinity of the driven electrode and had acquired enough energy in the driven electrode sheath to cross the plasma and reach the grounded electrode.

2.4.7 Time-resolved mass spectrometry

Since many discharges are now operated in the pulse regime, it is becoming increasingly important to understand the time variation of the concentrations and energies of ionic species. This is particularly important for the low-pressure pulsed plasma polymerisation of organic monomers to form thin films (Han *et al.*, 1998) and in the reactive pulsed magnetron sputtering of ceramic films (Vlček *et al.*, 2004).

There are essentially two methods to achieve time-resolution: (i) allow ions to continually enter the instrument and gate the detector signal (Hiden) or (ii) physically or electrically gate the ions entering the instrument and detect the arriving ion packets at the detector. The latter has been achieved on RF plasma reactors in inert gases and also in polymerising gases such as acrylic acid (Voronin *et al.*, 2005), and on magnetrons (Karkari *et al.*, 2002). In the latter, a time resolution of 4 μs was achieved using electronic gating.

2.5 Optical emission spectroscopy

In general, radiation emitted from plasma sources is either continuum or line radiation. Continuum radiation results from free–free (e.g. Bremsstrahlung) and free–bound (e.g. radiative recombination) interactions with the free electrons. In both cases the radiation depends, amongst other factors, on the continuous distribution of electron energies in the plasma. Line radiation results from photons emitted by electron transitions (bound–bound) between the discrete energy levels of the parent atom, molecule or ion. An electron in an upper level of energy, E_p, can spontaneously decay to a lower level, E_q, emitting a photon of energy $h\nu_{p,q} = E_p - E_q$. The spontaneous transition probability per second (one of the Einstein coefficients) is denoted by $A_{p,q}$ and its reciprocal is the mean life-time of the state. The number of electrons in a given level is determined by a balance between 'upward' processes (ionisation, excitation) and 'downward' processes (recombination, de-excitation). Plasmas in which radiative processes dominate (e.g. photo-ionisation, radiative recombination) are called radiative plasmas whereas collisional processes (e.g. impact ionisation and excitation) dominate in collisional plasmas, and this is usually the case in technological plasmas.

Plasmas in which radiation is completely re-absorbed (resonant radiation) are optically thick and have a large optical depth. The observed radiation provides information about the outer plasma regions only. In optically thin plasmas, re-absorption is insignificant so that radiation from the inner regions of the plasma can escape. Radiation from optically thin plasmas

offers insight into the dynamic and complicated atomic processes taking place deep within the plasma volume. The observed intensity (defined as the radiant energy dE emanating from an area dA in a time dt into a solid angle dΩ and has units of $\mathrm{J\,s^{-1}\,m^{-2}\,sr^{-1}}$) is then related to the electron density N_{p}^{z} of level p in a radiator of ionisation stage z (where $z = 0$ is neutral, 1 is singly ionised, etc.), the transition probability $A_{\mathrm{p,q}}$ and the thickness (D) of the plasma volume being observed:

$$I_{\mathrm{p,q}}^{z} = \frac{g(\nu_{\mathrm{p,q}})}{4\pi}\int_{0}^{D} N_{\mathrm{p}}^{z} A_{\mathrm{p,q}} h\nu_{\mathrm{p,q}}\,\mathrm{d}x \qquad [2.8]$$

Here, $g(\nu_{\mathrm{p,q}}) = TC_{\mathrm{f}}$ with C_{f} the wavelength dependant spectrometer calibration factor and T the window (or filter) transmission. The calibration factor is usually determined from a known black or grey body radiator such as a tungsten lamp. Usually it is necessary to assume a homogeneous plasma of depth D along the line-of-sight so that Equation 2.8 simplifies to $I_{\mathrm{p,q}}^{z} = [g(\nu_{\mathrm{p,q}})/4\pi]N_{\mathrm{p}}^{z}A_{\mathrm{p,q}}h\nu_{\mathrm{p,q}}D$. By comparison of the measured intensity–wavelength spectrum with a database of known emission lines, radical plasma species can be identified (e.g. Chaivan *et al.*, 2005). Since $I_{\mathrm{p,q}}^{z} \propto N_{\mathrm{p}}^{z}$, a qualitative measure of the radical density over a range of plasma conditions can also be obtained (e.g. Raffaele *et al.*, 2003).

This section attempts to cover some of the important aspects of optical emission spectroscopy (OES) and its use as a diagnostic. More thorough treatments can be found in McWhirter (1965), Cooper (1966), Richter (1968) and Lochte-Holtgreven (1968). For line broadening mechanisms, Wiese (1965) and Traving (1968) provide a comprehensive review. Other topics such as trace rare gases OES (Donnelly, 2004) and atmospheric plasma OES (Laux *et al.*, 2003) are treated elsewhere. Spectroscopic data useful to OES can be obtained from the NIST database (http://www.nist.gov).

2.5.1 Plasma models

To extract meaningful information from intensity measurements, spectroscopic models, which attempt to describe the main atomic processes in a plasma volume, are used. From these models, relationships between measured spectroscopic quantities such as line ratios or absolute intensities of selected emission lines enable the plasma parameters to be determined. In the following models, it is convenient to assume that the electrons have a Maxwellian energy distribution. Since many plasmas are non-Maxwellian, the electron temperature, T_{e}, is a characteristic temperature. Finally, it is assumed that the plasma being modelled is optically thin.

Steady-state corona model

At low pressures and electron plasma densities, N_{eo}, three-body recombination ($\propto N_{eo}^2$) and collisional de-excitation rates can become less than radiative recombination ($\propto N_{eo}$) and spontaneous emission. Also, collisional ionisation and excitation rates can dominate over radiative excitation and photo-ionisation. Under these conditions, collisional excitation (and ionisation) is balanced by spontaneous emission (and radiative recombination) to any lower level. Further simplification is achieved by considering only the dominant excitations from ground states and transitions between ground state ionisation stages. Finally, steady state is ensured by the population densities being in equilibrium with the slowly varying plasma parameters. Corona equilibrium is then defined by:

$$N_{eo}N_g^z X(T_e, g, p) = N_p^z \sum_{q<p} A(p, q) \qquad [2.9]$$

$$N_{eo}N_g^z S(T_e, z, g) = N_{eo}N_g^{z+1}\alpha(T_e, z+1, g) \qquad [2.10]$$

where X, S and α are the excitation, ionisation and radiative recombination coefficients respectively, with g representing the ground level. By substituting Equation 2.9 into 2.8, the observed intensity is then related to the population density N_p^z by

$$I_{p,q}^z = \frac{g(\nu_{p,q})}{4\pi} \int N_{eo}N_g^z X(T_e, g, p) h\nu_{p,q} R_{p,q} \mathrm{d}x \qquad [2.11]$$

where $R_{p,q} = A_{p,q} \Big/ \sum_{q<p} A_{p,q}$ is the branching ratio.

A common application of the corona model is to determine T_e by the ratio of line intensities. Lines are chosen so that the excitation coefficients are sufficiently different from each other and for this reason ionic to neutral ratios are preferred. For a homogeneous plasma and using Equation 2.11, this ratio is given by

$$\frac{I_{p,q}^{z+1}}{I_{k,l}^z} = \frac{g(\nu)_{p,q}}{g(\nu)_{k,l}} \frac{N_g^{z+1}}{N_g^z} \frac{X(T_e, g, p)\nu_{p,q}}{X(T_e, g, k)\nu_{k,l}} \frac{R_{p,q}}{R_{k,l}} \qquad [2.12]$$

The instrumental calibration factors can be cancelled out if the line wavelengths are close enough. Substituting $N_g^{z+1} / N_g^z = S / \alpha$ Equation 2.10 and known expressions for the coefficients X, S and α (McWhirter, 1965) into the above equation yields

$$\frac{I_{p,q}^{z+1}}{I_{k,l}^z} = C^* T_e^{3/4} \exp\left(-\frac{E_i^z + E_p - E_k}{kT_e}\right) \qquad [2.13]$$

with $C^* = (g_{p,q} / g_{k,l})C$. Here E_i^z is the neutral ($z = 0$) ionization potential, $E_{p,k}$ are energies of levels p and k (relative to the ground state) and C is a constant containing the spectroscopic information (Desai *et al.*, 1995). The constant C^* can be determined either by calculation (Desai *et al.*, 1995) (with known instrumental factors) or experimentally by calibrating this expression with, for example, T_e obtained from Langmuir probe measurements (Hope *et al.*, 1987; Desai *et al.*, 1995). In an extension of the line-ratio method, Samsonov and Goree (1999) used 2-D imaging to obtain temperature maps of a RF plasma. Further improvements to the line-ratio method, including using neutral line ratios, can be found in Boffard *et al.* (2004).

Collisional radiative model

At higher pressures and plasma densities, collisional de-excitation can compete with spontaneous emission. Under these conditions

$$\sum_{m<p} A(p, m) \leq N_{eo} X(T_e, q, p) \qquad [2.14]$$

and the corona model is invalid. Additionally, step-wise collision processes, transitions via neighbouring levels and metastable states are neglected in the model.

The collisional radiative model (CR) attempts to overcome some of these restrictions by considering: (i) ionisation by electron impact (from any bound level) balanced by three-body and radiative recombination and (ii) transitions between bound levels by electron collisions and radiative transitions to the lower levels. Due to its complexity, the CR model is not discussed in detail here and further information can be found in McWhirter (1965), Benoy *et al.* (1991), Bogaerts *et al.* (1998) and Kano *et al.* (2000). Various CR models have been developed for low pressure discharges (Vlček and Pelikán, 1989), atmospheric discharges (Vlček and Pelikán, 1990), inductively coupled plasmas (Vlček and Pelikán, 1991), microwave (Alves *et al.*, 1992) and magnetron plasmas (Trennepohl *et al.*, 1996; Debal *et al.*, 1998; Guimarães *et al.*, 1993). An important aspect of the CR model can be inferred from Equation 2.14 towards the higher levels. As $A(p,m)$ decreases and X increases (due to closer energy level spacing), there will be a level p* where the corona model becomes invalid even at low pressures. The population densities for levels higher than p* will be in approximate local thermodynamic equilibrium (LTE) with the lower energy free electrons. The densities of levels p and q (where $p > q$) are then determined by the Boltzmann relation:

$$\frac{N_p}{N_q} = \frac{\omega_p}{\omega_q} \exp\left(-\frac{\left(E_p - E_q\right)}{k_B T_{exe}} \right) \qquad [2.15]$$

where T_{exe} is the excitation temperature and ω_q is the statistical weight (i.e. the number of states in the qth level).

By using Equations 2.8, 2.15 and the absorption oscillator strength, defined by $f_{p,q} = (M_e c^3/8\pi^2 e^2 \nu_{p,q}^2)(\omega_p/\omega_q)A_{p,q}$, it can be shown that:

$$\frac{I_{p,q}\lambda_{p,q}^3}{f_{p,q}\omega_q} = \left(\frac{8\pi^2 e^2 h}{M_e}\right)\frac{N_q}{\omega_q} e^{-\frac{E_p - E_q}{k_B T_{exe}}} \qquad [2.16]$$

Also, by considering transitions that fall onto the same level q and taking logarithms, the above equation reduces to:

$$\ln\left(\frac{I_{p,q}\lambda_{p,q}^3}{f_{p,q}\omega_q}\right) = \ln\left(\frac{8\pi^2 eh}{M_e}\frac{N_q}{\omega_q} e^{-\frac{E_q}{k_B T_{exe}}}\right) - \frac{E_p}{k_B T_{exe}} \qquad [2.17]$$

A plot of $\ln(I_{p,q}\lambda_{p,q}^3/f_{p,q}\omega_q)$ against E_p, called a Boltzmann plot, then yields a straight line of gradient $-1/k_B T_{exe}$. Tabulated values for $\lambda_{p,q}$, $f_{p,q}$ and ω_q can then be used with the measured $I_{p,q}$ to determine the excitation temperature. Since the vibrational states in molecules also follow the Boltzmann distribution, this procedure can be also used to measure the vibrational temperature. In this case, the Einstein coefficient $A_{p,q}$ is replaced by the Frank–Condon factors for vibrational transitions (Iza and Hopwood, 2004). The Bolztmann plot can also be used to obtain the rotational temperature, which describes the population of rotational states in molecules; however, the procedure differs from above as the rotational states follow a modified Boltzmann distribution (Motret *et al.*, 2000; Iza and Hopwood, 2004).

2.5.2 Line broadening

Spectral line profiles do not have infinitesimal spectral width due to the emitter's interaction with the surrounding medium. The resulting broadening of the spectral lines, when combined with the appropriate theory, can be useful for plasma diagnostics. Pressure broadening results from interactions of the emitters with neighbouring neutral and ionised particles and generally depends on temperature and pressure. Interactions with neutral particles (resonant and Van der Waals broadening) are usually insignificant compared to charged particles (Stark broadening) if the fraction of ionised particles is $\geq -10^{-4}$. Instrumental broadening, due to the finite resolution of the spectrometer, can also contribute to the observed line shape. For atmospheric air plasmas with plasma densities $N_{eo} < 10^{21}\,m^{-3}$ Van der Waals broadening can be significant. Natural broadening, which results from interaction with electromagnetic fields causing energy levels to have a spread in energy, is usually negligible compared with the other broadening mechanisms. Line shapes arising from the different broadening mechanisms are

either Gaussian (instrumental, Doppler) or Lorentzian (Stark, Van der Waals, resonance, natural). An observed profile which contains Gaussian and Lorentzian elements is called a Voigt profile. If some of these elements are known, either theoretically or experimentally, they can be de-convolved from the Voigt profile to reveal the underlying line shape. Finally, broadening due to re-absorption of lines is usually negligible in low temperature plasmas. In plasma diagnostics, Doppler and Stark broadening are often the most useful and only these will be considered here.

Doppler broadening

The motion of an emitter relative to an observer causes the wavelength λ to be shortened or lengthened, with the shift being proportional to its velocity. The combined Doppler shifts over a velocity distribution of emitters then give rise to line broadening. For a Maxwellian distribution, the peak's full width at half maximum (FWHM) is given by $\Delta\lambda_{1/2} = 7.16 \times 10^{-7}\lambda(T/M)^{1/2}$ where T is the temperature (in Kelvins) and M is the atomic weight (in a.m.u.). Thermal Doppler broadening is then most pronounced for the lighter elements, particularly for hydrogen. If the other broadening mechanisms, such as Stark broadening, can be neglected or accounted for, then measurements of the FWHM immediately give the emitter temperature. In pure hydrogen RF discharges, Doppler broadening of the H_α line (656.28 nm) can reveal features relating to dissociative excitation and ionisation by electron impact of H_2 and fast excited H neutrals (Radovanov *et al.*, 1995). The ionic mobility and plasma electric field can also be inferred from Doppler shifts by using velocity modulation laser spectroscopy (Radunsky and Saykally, 1988) or two-beam Doppler shift laser spectroscopy (Sassi and Daily, 1988).

Stark broadening

Stark broadening is the result of two mechanisms: (i) the combined shifting of spectral lines caused by the nearest neighbour electric fields of the slower positive ions and (ii) fast electron collisions that interrupt the otherwise unperturbed photon wave train. The shifting of spectral lines due to electric fields, called the Stark effect, is more pronounced for the higher energy levels. Under comparable conditions, some of the most strongly broadened lines are those of H, He^+, Ar^+ and O^+ in which the Stark shift is linear with electric field (linear Stark effect). For other elements the Stark effect is quadratic with electric field (quadratic Stark effect) and broadening is smaller. For hydrogen, the spectral shifts are symmetrical with no net shift whereas for other elements shifting as well as broadening is observed. The theory of Stark broadening is extremely complicated but approximate

formulae can be derived that relate the line width to the plasma density for lines with weak temperature dependence. In this case the H_β (486.13 nm) Balmer line is particularly useful because good agreement between theory and experiment have been obtained, and the FWHM is related to the plasma density by the formulae $\Delta\lambda_{1/2} = 0.040 N_{eo}^{2/3}$ nm where N_{eo} is in units of $10^{20}\,m^{-3}$. The temperature dependence of the H_γ (434.05 nm) line is more pronounced and Torres *et al.* (2006) exploited this, with measurements of the FWHM of both lines, to obtain the electron density and temperature from an atmospheric microwave discharge. In strong electric fields (~ kV/cm), Stark splitting of the H_α (656.28 nm) line can be used to measure the electric field strength. Wujec *et al.* (2003) applied this technique to a hydrogen dielectric barrier discharge at low pressure (~ kPa). In an atmospheric dielectric barrier discharge, Dong *et al.* (2005) used Stark broadening to obtain the micro-discharge electron density. In plasmas in which the Balmer lines are a convolution of Doppler-broadened and Stark-shifted profiles, electric fields can still be determined (Barbeau and Jolly, 1991).

2.5.3 Abel inversion

Abel inversion is a powerful method where line-of-sight intensity measurements can give information on the internal radial distribution of the plasma emissivity, $\varepsilon(r)$. This is defined as the radiant energy emitted from a volume dV per unit time into a solid angle $d\Omega$. In general, emissivity is a function of position and direction and is closely related to intensity. The method is illustrated in Fig 2.11 in which a plasma slice is shown. Here $I(y)$ is the total intensity emitted by the plasma column of width dy at y, where distances

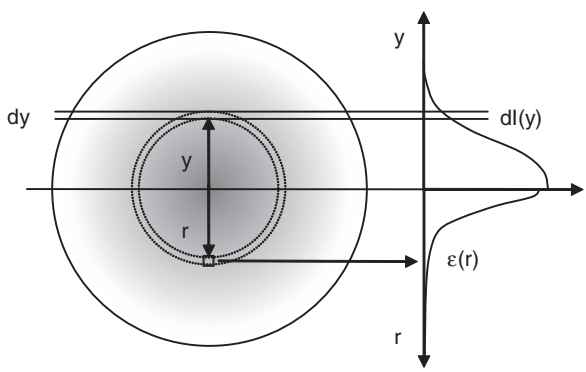

2.11 Schematic of a radially symmetric optically thin plasma. The observed intensity dI(y) is the total intensity from the plasma column of width dy. Integration of $[dI(y)/dy]\,(y^2 - r^2)^{-1/2}\,dy$ from y = r to the plasma edge (at y = 1) is related, by Abel inversion, to the radial emissivity ε(r).

are normalised to the plasma edge ($y = 1$). If the plasma is optically thin, has axial symmetry and $I(y = 1) = 0$ outside the plasma, then the intensity is related to the emissivity by Abel's inversion equation:

$$\varepsilon(r) = -\frac{1}{\pi}\int_{r=y}^{1}\frac{\mathrm{d}I(y)}{\mathrm{d}y}\frac{\mathrm{d}y}{\left(y^2 - r^2\right)^{1/2}} \qquad [2.18]$$

The evaluation of this equation is not trivial since there are two main problems associated with the integral. Firstly, the derivative tends to amplify any inherent noise in the experimental data so that prior smoothing is necessary. Secondly, the integral exhibits a singularity at $y = r$ introducing significant errors at the start of integration. Errors can also occur when $\mathrm{d}I(y)/\mathrm{d}y \to 0$ at the axis of symmetry and at $y \approx 1$ (and are called termination errors). The evaluation of this integral using a direct approach usually yields unacceptable errors so more sophisticated techniques, such as polynomial fitting (Cremers and Birkebak, 1966), iteration (Vicharelli and Lapatovich, 1987), transform techniques (Smith and Keefer, 1988) and cubic splines (Gueron and Deutsch, 1994), are used.

2.6 References

Introduction

Becker K H, Kogelschatz U, Schoenbach K H and Barker R J (2005), *Non-equilibrium Air Plasma at Atmospheric Pressure*, Bristol, IOP Publishing.

Biederman H (2004), *Plasma Polymer Films*, London, Imperial College Press.

Hippler R, Pfau S, Schmidt M and Schoenbach K H (2000), *Low Temperature Plasma Physics*, Berlin, Wiley-VCH Verlag.

Hutchinson I H (1994), *Principles of Plasma Diagnostics*, Cambridge, Cambridge University Press.

Ovsyannikov A A and Zhukov M F (2000), *Plasma Diagnostics*, Cambridge, Cambridge International Science Publishing.

Discharge electrical characteristics

Bakker L P, Kroesen G M W and de Hoog F J (1999), 'RF discharge impedance measurements using a new method to determine the stray impedances', *IEEE Trans. Plasma Sci.*, **27**, 759–765.

Borcia G, Anderson C A and Brown N M D (2003), 'Dielectric barrier discharge for surface treatment: application to selected polymers in film and fibre form', *Plasma Sources Sci. Technol.*, **12**, 335–344.

Borcia G, Anderson C A and Brown N M D (2005), 'Using a nitrogen dielectric barrier discharge for surface treatment', *Plasma Sources Sci. Technol.*, **14**, 259–267.

Bose F, Patrick R and Baltes H P (1994), 'Characterization of plasma etch processes using measurements of discharge impedance', *J. Vac. Sci. Technol. B*, **12**, 2805–2809.

Braithwaite N St J (1997), 'Internal and external electrical diagnostics of RF plasmas', *Plasma Sources Sci.Technol.*, **6**, 133–139.

Dewan M N A, McNally P J, Perova T and Herbert P A F (2001), 'Use of plasma impedance monitoring for the determination of SF_6 reactive ion etch process end points in a SiO_2/Si system', *Mat. Res. Innov.*, **5**, 107–116.

Falkenstein Z and Coogan J J (1997), 'Microdischarge behaviour in the silent discharge of nitrogen–oxygen and water–air mixtures', *J. Phys. D: Appl. Phys.*, **30**, 817–825.

Hargis P J, Greenberg K E, Miller P A, Gerardo J B, Torczynski J R, Riley M E, Hebner G A, Roberts J R, Olthoff J K, Whetstone J R, Van Brunt R J, Sobolewski M A, Anderson H M, Splichal M P, Mock J L, Bletzinger P, Garscadden A, Gottschco R A, Selwyn G, Dalvie M, Heidenreich J E, Butterbaugh J W, Brake M L, Passow M L, Pender J, Lujan A, Elta M E, Graves D B, Sawin H H, Kushner M J, Verdeyen J T, Horwath R and Turner T R (1994), 'The Gaseous Electronics Conference Radiofrequency reference cell – A defined parallel-plate radio-frequency system for experimental and theoretical studies of plasma processing discharges', *Rev. Sci. Instrum.*, **65**, 140–154.

Lieberman M and Lichtenberg A (1994), *Principles of Plasma Discharges and Materials Processing*, New York, Wiley.

Sira M, Trunec D, Stahel P, Bursıkova V, Navratil Z and Bursık J (2005), 'Surface modification of polyethylene and polypropylene in atmospheric pressure glow discharge', *J. Phys. D: Appl. Phys.*, **38**, 621–627.

Sobolewski M A (1992), 'Electrical characterization of radiofrequency discharges in the gaseous electronics conference reference cell', *J. Vac. Sci.Technol. A*, **10**, 3550–3562.

Teuner D, Lücking C and Mentel J (1999), 'Electrical characterisation of capacitive RF discharges', *Proc. ICPIG XXIV*, **1**, 145.

Electrical plasma diagnostics

Aikawa H (1976), 'Measurement of anisotropy of electron-distribution function of a magnetized plasma', *J. Phys. Soc. Japan*, **40**, 1741–1749.

Alami J, Gudmundsson J T, Bohlmark J, Birch J and Helmersson U (2005), 'Plasma dynamics in a highly ionized pulsed magnetron discharge', *Plasma Sources Sci. Technol.*, **14**, 525–531.

Allen J E (1992a), 'Probe theory – the orbital motion approach', *Physica Scripta*, **45**, 497–503.

Allen J E (1992b), 'On the plotting of electron and ion distribution functions', *J. Phys. D: Appl. Phys.*, **25**, 1839–1840.

Allen J E, Boyd R L F and Reynolds P (1957), 'The collection of positive ions by a probe immersed in a plasma', *Proc. Phys. Soc. B*, **70**, 297–304.

Amemiya H (1986), 'Experiments on the energy-distribution function in hydrogen plasmas', *Jap. J. Appl. Phys.*, **25**, 595–600.

Amemiya H (1990), 'Plasmas with negative ions – probe measurements and charge equilibrium', *J. Phys. D: Appl. Phys.*, **23**, 999–1014.

Amemiya H and Yasuda N (1997), 'Capacitive radio frequency discharge plasma containing negative ions', *J. Phys. Soc. Japan*, **66**, 623–632.

Amemiya H, Annaratone B M and Allen J E (1999), 'The collection of positive ions by spherical and cylindrical probes in an electronegative plasma', *Plasma Sources Sci. Technol.*, **8**, 179–190.

Annaratone B M, Allen M W and Allen J E (1992), 'Ion currents to cylindrical Langmuir probes in RF plasmas', *J. Phys. D: Appl. Phys.*, **25**, 417–424.

Annaratone B M and Braithwaite N St J (1991), 'A comparison of a passive (filtered) and an active (driven) probe for RF plasma diagnostics', *Meas. Sci. Technol.*, **2**, 795–800.

Böhm C and Perrin J (1993), 'Retarding-field analyzer for measurements of ion energy distributions and secondary electron emission coefficients in low-pressure radio frequency discharges', *Rev. Sci. Instrum.*, **64**, 31–44.

Booth J P, Braithwaite N St J, Goodyear A and Barroy P (2000), 'Measurements of characteristic transients of planar electrostatic probes in cold plasmas', *Rev. Sci. Instrum.*, **71**, 2722–2727.

Boschi A and Magistrelli F (1963), 'Effect of an RF signal on the characteristic of a Langmuir probe', *Nuovo Cimento*, **29**, 487–499.

Bradley J W, Karkari S K and Vetushka A (2004), 'A study of the transient plasma potential in a pulsed bi-polar dc magnetron discharge', *Plasma Sources Sci. Technol.*, **13**, 189–198.

Braithwaite N St J and Allen J E (1988), 'Boundaries and probes in electronegative plasmas', *J. Phys. D: Appl. Phys.*, **21**, 1733–1737.

Bryant P, Dyson A and Allen J E (2001a), 'Langmuir probe measurements of weakly collisional electropositive RF discharge plasmas', *J. Phys. D: Appl. Phys.*, **34**, 1491–1498.

Bryant P, Dyson A and Allen J E (2001b), 'Langmuir probe measurements of weakly collisional electronegative RF discharge plasmas', *J. Phys. D: Appl. Phys.*, **34**, 95–104.

Bryant P (2003), 'Floating potential of spherical probes and dust grains in collisional plasmas', *J. Phys. D: Appl. Phys.*, **36**, 2859–2868.

Chabert P, Sheridan T E, Boswell R W and Perrin J (1999), 'Electrostatic probe measurement of the negative ion fraction in an SF_6 helicon discharge' *Plasma Sources Sci. Technol.*, **8**, 561–566.

Chatterton P A, Rees J A, Wu W L and Al-Assadi K (1991), 'A self-compensating Langmuir probe for use in rf (13.56 MHz) plasma systems', *Vacuum*, **42**, 489–493.

Chen F F (1965a), 'Electric probes', in Huddlestone R H and Leonard S L (eds), *Plasma Diagnostic Techniques*, New York, Academic Press, 113–200.

Chen F F (1965b), 'Numerical computations for ion probe characteristics in a collisionless plasma', *J. Nucl. Energy, Part C*, **7**, 47–67.

Chen F F (2001), 'Langmuir probe analysis for high density plasmas', *Phys. Plasmas*, **8**, 3029–3041.

Chou Y S, Talbot L and Willis D R (1966), 'Kinetic theory of a spherical electrostatic probe in a stationary plasma', *Phys. Fluids*, **9**, 2150–2167.

Chung P M, Talbot L and Touryan K J (1975), *Electric Probes in Stationary and Flowing Plasmas: Theory and Application*, New York, Springer.

Cohen I M (1963), 'Asymptotic theory of spherical electrostatic probes in a slightly ionized, collision-dominated gas', *Phys. Fluids*, **6**, 1492–1499.

Demidov V I, Ratynskaia S V and Rypdal K (2002), 'Electric probes for plasmas: The link between theory and instrument', *Rev. Sci. Instrum.*, **73**, 3409–3439.

DeNeef C P and Theiss A J (1979), 'Effect of finite analyzer size on the distribution functions measured in field-free plasmas', *Rev. Sci. Instrum.*, **50**, 378–381.

Donoso G and Martin P (1986), 'Grid effects on velocity analyzers of variable geometry', *Rev. Sci. Instrum.*, **57**, 1501–1506.

Donoso G and Martin P (1990), 'Space-charge effects in a velocity analyzer of variable geometry', *Rev. Sci. Instrum.*, **61**, 3381–3383.

Dyson A, Bryant P and Allen J E (2000), 'Multiple harmonic compensation of Langmuir probes in rf discharges', *Meas. Sci. Technol.*, **11**, 554–559.

Edelberg E A, Perry A, Benjamin N and Aydil E S (1999a), 'Energy distribution of ions bombarding biased electrodes in high density plasma reactors', *J. Vac. Sci. Technol. A*, **17**, 506–516.

Edelberg E A, Perry A, Benjamin N and Aydil E S (1999b), 'Compact floating ion energy analyzer for measuring energy distributions of ions bombarding radio-frequency biased electrode surfaces', *Rev. Sci. Instrum.*, **70**, 2689–2698.

Enloe C L and Shell J R (1992), 'Optimizing the energy resolution of planar retarding potential analyzers', *Rev. Sci. Instrum.*, **63**, 1788–1791.

Flender U and Wiesemann K (1994), 'Ion distribution functions behind an rf sheath', *J. Phys. D: Appl. Phys.*, **27**, 509–521.

Fujita F and Yamazaki H (1990), 'Determination of electron energy distribution function of plasmas by digital processing from Langmuir probe characteristic', *Jap. J. Appl. Phys.*, **29**, 2139–2144.

Godyak V A, Piejak R B and Alexandrovich B M (1992), 'Measurements of electron energy distribution in low-pressure RF discharges', *Plasma Sources Sci. Technol.*, **1**, 36–58.

Hershkowitz N (1989), 'How Langmuir probes work', in Auciello O and Flamm D L (eds), *Plasma Diagnostics*, Volume 1, New York, Academic Press, 113–183.

Honzawa T, Sekizawa T, Miyauchi Y and Nagasawa T (1993), 'Effects of space charges in gridded energy analyzer', *Jpn. J. Appl. Phys.*, **32**, 5748–5753.

Hopkins M B and Graham W G (1986), 'Langmuir probe technique for plasma parameter measurement in a medium density discharge', *Rev. Sci. Instrum.*, **57**, 2210–2217.

Ingram S G, Annaratone B M and Ohuchi M (1990), 'Design and use of a gridded probe in a low-pressure rf argon discharge', *Rev. Sci. Instrum.*, **61**, 1883–1891.

Ingram S G and Braithwaite N St J (1988), 'Ion and electron energy analysis at a surface in an rf discharge', *J. Phys. D: Appl. Phys.*, **21**, 1496–1503.

Iwama N, Lehner T, Noziri H and Okado M (1988), 'Three-dimensional reconstruction of the ion velocity distribution function of plasma with a retarding-grid analyzer', *Appl. Phys. Lett.*, **52**, 96–97.

Kamitsuma M, Chen S L and Chang J S (1977), 'The theory of the instantaneous triple-probe method for direct-display of plasma parameters in low-density collisionless plasmas', *J. Phys. D: Appl. Phys.*, **10**, 1065–1077.

Kamitsuma M and Teii S (1982), 'Theory of a spheroidal probe in low-density continuum plasmas', *Phys. Fluids*, **25**, 1169–1173.

Kennedy R V and Allen J E (2003), 'The floating potential of spherical probes and dust grains. II: Orbital motion theory', *J. Plasma Physics*, **69**, 485–506.

Kimura T, Yoneya A and Ohe K (1991), 'Detection of electron energy distribution function by finite impulse response filter', *Jap. J. Appl. Phys.*, **8**, 1877–1881.

Klagge S and Lunk A (1991), 'Probe diagnostics of anisotropic plasma in a hollow cathode arc', *J. Appl. Phys.*, **70**, 99–105.

Kono A (2003), 'Intrinsic sheath edge conditions for sheath instability in low-pressure electronegative plasmas', *J. Phys. D: Appl. Phys.*, **36**, 465–472.

Kortshagen U and Zethoff M (1995), 'Ion energy distribution functions in a planar inductively coupled rf discharge', *Plasma Sources Sci. Technol.*, **4**, 541–550.

Liu J, Huppert G L and Sawin H H (1990), 'Ion bombardment in rf plasmas', *J. Appl. Phys.*, **68**, 3916–3934.

Mezentsev A P, Mustafaev A S and Fedorov V L (1988), 'Probe measurements of the electron convective velocity in axisymmetric low-temperature helium plasmas', *J. Phys. D: Appl. Phys.*, **21**, 1464–1466.

Moskalev I N (1970), 'Influence of the first grid on the characteristics of a multigrid energy analyzer', *Sov. Phys. Tech. Phys.*, **15**, 371–376.

Niyogi K K and Cohen I M (1973), 'Continuum electrostatic probe theory with magnetic field', *Phys. Fluids*, **16**, 69–74.

Palop J I F, Ballesteros J, Colomer V and Hernández M A (1995), 'A new smoothing method for obtaining the electron energy distribution function in plasmas by the numerical differentiation of the I–V probe characteristic', *Rev. Sci. Instrum.*, **66**, 4625–4636.

Passoth E, Kudrna P, Csambal C, Behnke J F, Tichý M and Helbig V (1997), 'An experimental study of plasma density determination by a cylindrical Langmuir probe at different pressures and magnetic fields in a cylindrical magnetron discharge in heavy rare gases', *J. Phys. D: Appl. Phys.*, **30**, 1763–1777.

Piejak R B, Al-Kuzee J and Braithwaite N St J (2005), 'Hairpin resonator probe measurements in rf plasmas', *Plasma Sources Sci. Technol.*, **14**, 734–743.

Riemann K U (1991), 'The Bohm criterion and sheath formation', *J. Phys. D: Appl. Phys.*, **24**, 493–518.

Rubinstein J and Laframboise J G (1983), 'Theory of axially symmetric probes in a collisionless magnetoplasma: aligned spheroids, finite cylinders, and disks', *Phys. Fluids*, **26**, 3624–3627.

Sanmartin J R (1970), 'Theory of a probe in a strong magnetic field', *Phys. Fluids*, **13**, 103–116.

Sakai Y and Katsumata I (1985), 'An energy resolution formula of a three plane grid retarding field energy analyzer', *Jap. J. Appl. Phys.*, **24**, 337–341.

Schott L (1968), 'Electrical probes', in Lochte-Holtgreven W (ed.), *Plasma Diagnostics*, Amsterdam, North Holland Publishing Company, 668–731.

Self S A and Shih C H (1968), 'Theory and measurements for ion collection by a spherical probe in a collisional plasma', *Phys. Fluids*, **11**, 1532–1545.

Shih C H and Levi E (1971), 'The effect of collisions on cold ion collection by means of Langmuir probes', *AIAA J.*, **9**, 1673.

Simpson J A (1961), 'Design of retarding field energy analyzers', *Rev. Sci. Instrum.*, **32**, 1283–1293.

Sonmor L J and Laframboise J G (1991), 'Exact current to a spherical electrode in a collisionless, large-Debye-length magnetoplasma', *Phys. Fluids B*, **3**, 2472–2490.

Sowa M J, Blain M G, Jarecki R L and Stevens J E (2002), 'Spatially resolved electron temperature measurements with a microfabricated retarding field analyser', *Appl. Phys. Lett.*, **80**, 932–934.

Stangeby P C and Allen J E (1971), 'Transonic plasma flow past an obstacle', *J. Plasma Phys.*, **6**, Part 1, 19–32.

Stenzel R L, Gekelman W, Wild N, Urrutia J M and Whelan D (1983), 'Directional velocity analyzer for measuring electron distribution functions in plasmas', *Rev. Sci. Instrum.*, **54**, 1302–1310.

Su C H and Lam S H (1963), 'Continuum theory of spherical electrostatic probes', *Phys. Fluids*, **6**, 1479–1491.

Sudit I D and Woods R C (1994), 'A study of the accuracy of various Langmuir probe theories', *J. Appl. Phys.*, **76**, 4488–4498.

Swift J D and Schwar M J R (1970), *Electrical Probes for Plasma Diagnostics*, London, Iliffe.

Thompson S M and Bradley J W (2001), 'The effect of rotating cylindrical Langmuir probes in magnetron plasmas', *Contrib. Plasma Phys.*, **41**, 481–487.

Thompson B E, Allen K D, Richards A D and Sawin H H (1986), 'Ion bombardment energy distributions in radio-frequency glow-discharge systems', *J. Appl. Phys.*, **59**, 1890–1903.

Tichý M, Šícha M, David P and David T (1994), 'A collisional model of the positive ion collection by a cylindrical Langmuir probe', *Contrib. Plasma Phys.*, **34**, 59–68.

Welzel Th., Dunger Th., Kupfer H and Richter F (2004), 'A time-resolved Langmuir double-probe method for the investigation of pulsed magnetron discharges', *J. Appl. Phys.*, **96**, 6994–7001.

Woodworth J R, Abraham I C, Riley M E, Miller P A, Hamilton T W, Aragon B P, Shul R J, and Willison C G (2002), 'Ion energy distributions at rf-biased wafer surfaces', *J. Vac. Sci. Technol. A*, **20**, 873–886.

Plasma mass spectrometry

Barton D, Heason D J, Short R D and Bradley J W (2000), 'The measurement and control of the ion energy distribution function at a surface in an RF plasma', *Meas. Sci. Technol.*, **11**, 1726–1731.

Barton D, Short R D, Fraser S and Bradley J W (2003), 'The effect of ion energy upon plasma polymerization deposition rate for acrylic acid', *Chem. Commun.*, **3**, 348–349.

Biederman H (2004), *Plasma Polymer Films*, London, Imperial College Press.

Brink G O (1966), 'Electron bombardment molecular beam detector', *Rev. Sci. Istrum.*, **37**, 857–860.

Coburn J W and Kay E (1971), 'Pressure considerations associated with ion sampling from glow discharges', *J. Vac. Sci. Technol.*, **8**, 738–743.

Dawson P H (1976), *Quadrupole Mass Spectrometry and its Applications*, Oxford, Elsevier.

Haddow D B, France R M, Short R D, Bradley J W and Barton D (2000), 'A mass spectrometric and ion energy study of the continuous wave plasma polymerization of acrylic acid', *Langmuir*, **16**, 5654–5660.

Han L C M, Timmons R B, Lee W W, Chen Y Y and Hu Z B (1998), 'Pulsed plasma polymerization of pentafluorostyrene: synthesis of low dielectric constant films', *J. Appl. Phys.*, **84**, 439–444.

Hiden, http://www.hidenanalytical.com.

Howling A A, Sansonnens L, Dorier J L and Hollenstein Ch (1993a), 'Negative hydrogenated silicon ion clusters as particle precursors in rf silane plasma deposition', *J. Phys D: Appl. Phys.*, **26**, 1003–1006.

Howling A A, Dorier J L and Hollenstein Ch (1993b), 'Negative-ion mass-spectra and particulate formation in radio-frequency silane plasma deposition experiments', *Appl. Phys. Lett.*, **62**, 1341–1343.

Janes J and Börnig K (1993), 'Energy distributions of argon neutrals at the rf-powered electrode of a parallel-plate reactor', *J. Appl. Phys.*, **73**, 2724–2731.

Jarvis K E, Gray A L, Williams J G (1990), *Plasma Source Mass Spectrometry*, Cambridge, Royal Society of Chemistry.

Kae-Nune P, Perrin J, Guillon J and Jolly J (1995), 'Mass-spectrometry detection of radicals in SiH_4–CH_4–H_2 glow-discharge plasmas', *Plasma Sources Sci. Technol.*, **4**, 250–259.

Karkari S K, Bäcker H, Forder D and Bradley J W (2002), 'A technique for obtaining time- and energy-resolved mass spectroscopic measurements on pulsed plasmas', *Meas. Sci. Technol.*, **13**, 1431–1436.

Kawamura E, Vahedi V, Lieberman M A and Birdsall C K (1999), 'Ion energy distributions in rf sheaths; review, analysis and simulation', *Plasma Sources Sci. Technol.*, **8**, R45–R64.

Kusano E, Kobayashi T, Kashiwagi N, Saitoh T, Saiki S, Nanto H and Kinbara A (1999), 'Ion energy distribution in ionized dc sputtering measured by an energy-resolved mass spectrometer', *Vacuum*, **53**, 21–24.

Lieberman M and Lichtenberg A (1994), *Principles of Plasma Discharges and Materials Processing*, New York, Wiley.

Liu J, Huppert G L and Sawin H H (1990), 'Ion bombardment in rf plasmas', *J. Appl. Phys.*, **68**, 3916–3934.

McDowell C A (1963), 'Types of mass spectrometers', in Farmer J B (ed.), *Mass Spectrometry*, New York, McGraw-Hill, 7–44.

Mišina M, Bradley J W, Bäcker H, Aranda-Gonzalvo Y, Karkari S K and Forder D (2003), 'Investigation of the pulsed magnetron discharge by time- and energy-resolved mass spectrometry', *Vacuum*, **68**, 171–181.

Overzet L J, Beberman J H and Verdeyen J T (1989), 'Enhancement of the negative-ion flux to surfaces from radio-frequency processing discharges', *J. Appl. Phys.*, **66**, 1622–1631.

Pecher P and Jacob W (1998), 'Determination of the absolute CH_3 radical flux emanating from a methane electron cyclotron resonance plasma', *Appl. Phys. Letts.*, **73**, 31–33.

Rees J A, Seymour D L, Greenwood C L and Scott A (1998), 'An improved method for the study of neutral species produced in processing plasmas', *Nucl. Inst. Meth. Phys. Res. B*, **134**, 73–76.

Riemann K U (1989), 'Theoretical analysis of the electrode sheath in rf discharges', *J. Appl. Phys.*, **65**, 999–1004.

Robertson R and Gallagher A (1986), 'Monosilicon and disilicon radicals in silane and silane–argon dc discharges', *J. Appl. Phys.*, **59**, 3402–3411.

Sasaki S, Ishikawa I, Nagaseki K, Saito Y and Suganomata S (1997), 'Positive and negative ions in RF plasmas of SF_6/N_2 and SF_6/Ar mixtures in a planar diode', *Jap. J. Appl. Phys.*, **36**, 847–853.

Schwarzenbach W, Tserepi A, Derouard J and Sadeghi N (1997), 'Mass spectrometric detection of F atoms and CF_x radicals in CF_4 plasmas', *Jpn. J. Appl. Phys.*, **36**, 4644–4647.

Singh H, Coburn J W and Graves D B (1999), 'Mass spectrometric detection of reactive neutral species: Beam-to-background ratio', *J. Vac. Sci. Technol. A*, **17**, 2447–2455.

Stoffels E, Stoffels W W and Tachibana K (1998), 'Electron attachment mass spectroscopy as a diagnostics for electronegative gases and plasmas', *Rev Sci. Inst.*, **69**, 116–122.

Vlček J, Pajdarova A D and Musil J (2004), 'Pulsed dc magnetron discharges and their utilization in plasma surface engineering', *Cont. Plasma Phys.*, **44**, 426–436.

Vohrer U, Muller M and Oehr C (1998), 'Glow-discharge treatment for the modification of textiles', *Surf. Coat. Technol.*, **98**, 1128–1131.

Voronin S A, Alexander M R and Bradley J W (2005), 'Time-resolved measurements of the ion energy distribution function in a pulsed discharge using a double gating technique', *Meas. Sci. Technol.*, **16**, 2446–2452.

White F A and Wood G M (1986), 'Types of Mass Spectrometers', in *Mass Spectrometry Applications in Science and Engineering*, New York, Wiley, 51–88.

Zeuner M (2004), in Biederman H (ed.), *Plasma Polymer Films*, London, Imperial College Press, Chapter 4.

Zeuner M, Meichsner J and Rees J A (1996), 'High energy negative ions in a radio-frequency discharge', *J. Appl. Phys.*, **79**, 9379–9381.

Zeuner M, Neumann H, Zalman J and Biederman H (1988), 'Sputter process diagnostics by negative ions', *J. Appl. Phys.*, **83**, 5083–5086.

Optical emission spectroscopy

Alves L L, Gousset G and Ferreira C M (1992), 'A collisional-radiative model for microwave discharges in helium at low and intermediate pressures', *J. Phys. D: Appl. Phys.*, **25**, 1713–1732.

Barbeau C and Jolly J (1991), 'Electric field measurement in the cathode sheath of a hydrogen glow discharge', *Appl. Phys. Lett.*, **58**, 237–239.

Benoy D A, van der Mullen J A M, van der Sude B and Schram D C (1991), 'A novel collisional radiative model with a numerical bottom and an analytical top', *J. Quant. Spectrosc. Radiat. Transfer*, **46**, 195–210.

Boffard J B, Lin C C and DeJoseph Jr C A (2004), 'Application of excitation cross sections to optical plasma diagnostics', *J. Phys. D: Appl. Phys.*, **37**, R143–R161.

Bogaerts A, Gijbels R and Vlček J (1998), 'Collisional-radiative model for an argon glow discharge', *J. Appl. Phys.*, **84**, 121–136.

Chaivan P, Pasaja N, Boonyawan D, Suanpoot P and Vilaithong T (2005), 'Low-temperature plasma treatment for hydrophobicity improvement of silk', *Surf. Coat. Technol.*, **193**, 356–360.

Cooper J (1966), 'Plasma spectroscopy', *Rep. Prog. Phys.*, **29**, 35–130.

Cremers C J and Birkebak R C (1966), 'Application of the Abel integral equation to spectrographic data', *Appl. Opt.*, **5**, 1057–1064.

Debal F, Bretagne J, Jumet M, Wautelet M, Dauchot J P and Hecq M (1998), 'Analysis of DC magnetron discharges in Ar-N_2 gas mixtures. Comparison of a collisional-radiative model with optical emission spectroscopy', *Plasma Sources Sci. Technol.*, **7**, 219–229.

Desai T M, Gogawale S V, Shukla A B, Joshi N K, Salgaonkar U S and Bhale G L (1995), 'Electron temperature measurements in uhv systems by spectroscopic and Langmuir probe techniques', *Vacuum*, **46**, 223–226.

Dong L F, Ran J X and Mao Z G (2005), 'Direct measurement of electron density in microdischarge at atmospheric pressure by Stark broadening', *Appl. Phys. Lett.*, **86**, 1501–1503.

Donnelly V M (2004), 'Plasma electron temperatures and electron energy distributions measured by trace rare gases optical emission spectroscopy', *J. Phys. D: Appl. Phys.*, **37**, R217–R236.

Gueron S and Deutsch M (1994), 'A fast Abel inversion algorithm', *J. Appl. Phys.*, **75**, 4313–4318.

Guimarães F, Almeida J B and Bretagne J (1993), 'Study of an argon magnetron discharge used for molybdenum sputtering. II: spectroscopic analysis and comparison with the model', *Plasma Sources Sci. Technol.*, **2**, 138–144.

Hope D A O, Cox T I and Deshmukh V G I (1987), 'Langmuir probe and optical emission spectroscopic studies of Ar and O_2 plasmas', *Vacuum*, **37**, 275–277.

Iza F and Hopwood J A (2004), 'Rotational, vibrational, and excitation temperatures of a microwave-frequency microplasma', *IEEE Trans. Plasma Sci.*, **32**, 498–504.

Kano K, Suzuki M and Akatsuka H (2000), 'Spectroscopic measurement of electron temperature and density in argon plasmas based on collisional-radiative model', *Plasma Sources Sci. Technol.*, **9**, 314–322.

Laux C O, Spence T G, Kruger C H and Zare R N (2003), 'Optical diagnostics of atmospheric pressure air plasmas', *Plasma Sources Sci. Technol.*, **12**, 125–138.

Lochte-Holtgreven W (1968), 'Evaluation of plasma parameters', in Lochte-Holtgreven W (ed.), *Plasma Diagnostics*, Amsterdam, North Holland, 135–213.

McWhirter R W P (1965), 'Spectral Intensities', in Huddlestone R H and Leonard S L (eds), *Plasma Diagnostics Techniques*, New York, Academic Press, 201–264.

Motret O, Hibert C, Pellerin S and Pouvesle J M (2000), 'Rotational temperature measurements in atmospheric pulsed dielectric barrier discharge – gas temperature and molecular fraction effects', *J. Phys. D: Appl. Phys.*, **33**, 1493–1498.

Radovanov S B, Dzierżega K, Roberts J R and Olthoff J K (1995), 'Time-resolved Balmer-alpha emission from fast hydrogen atoms in low pressure, radio-frequency discharges in hydrogen', *Appl. Phys. Lett.*, **66**, 2637–2639.

Radunsky M B and Saykally R J (1988), 'Non-intrusive measurement of axial electric fields in low-pressure glow discharges by velocity modulation laser spectroscopy', *Chem. Phys. Lett.*, **152**, 419–423.

Raffaele A A, Riccardi C, Selli E, Barni R, Piselli M, Poletti G, Orsini F, Marcandalli B, Massafra M R and Meda L (2003), 'Characterization of plasma processing for polymers', *Surf. Coat. Technol.*, **174–175**, 886–890.

Richter J (1968), 'Radiation of hot gases', in Lochte-Holtgreven W (ed.), *Plasma Diagnostics*, Amsterdam, North Holland, 1–65.

Samsonov D and Goree J (1999), 'Line ratio imaging of a gas discharge', *IEEE Trans. Plasma Sci.*, **27**, 76–77.

Sassi M and Daily J W (1988), 'Doppler shift methods for plasma diagnostics', *J. Quant. Spectrosc. Radiat. Transfer*, **40**, 429–437.

Smith L M and Keefer D R (1988), 'Abel inversion using transform techniques', *J. Quant. Spectrosc. Radiat. Transfer*, **39**, 367–373.

Torres J, van de Sande M J, van der Mullen J J A M, Gamero A and Sola A (2006), 'Stark broadening for simultaneous diagnostics of the electron density and temperature in atmospheric microwave discharges', *Spectrochimica Acta Part B*, **61**, 58–68.

Traving G (1968), 'Interpretation of line broadening and line shift', in Lochte-Holtgreven W (ed.), *Plasma Diagnostics*, Amsterdam, North Holland, 66–134.

Trennepohl Jr W, Bretagne J, Gousset G, Pagnon D and Touzeau M (1996), 'Modelling of an Ar-O_2 reactive magnetron discharge used for deposition of chromium oxide', *Plasma Sources Sci. Technol.*, **5**, 607–621.

Vicharelli P A and Lapatovich W P (1987), 'Iterative method for computing the inverse Abel transform', *Appl. Phys. Lett.*, **50**, 557–559.

Vlček J and Pelikán V (1989), 'A collisional-radiative model applicable to argon discharges over a wide range of conditions. II: Application to low-pressure, hollow-cathode arc and low-pressure glow discharges', *J. Phys. D: Appl. Phys.*, **22**, 632–643.

Vlček J and Pelikán V (1990), 'A collisional-radiative model applicable to argon discharges over a wide range of conditions. III: Application to atmospheric and subatmospheric pressure arcs', *J. Phys. D: Appl. Phys.*, **23**, 526–532.

Vlček J and Pelikán V (1991), 'A collisional-radiative model applicable to argon discharges over a wide range of conditions. IV: Application to inductively coupled plasmas', *J. Phys. D: Appl. Phys.*, **24**, 309–317.

Wiese W L (1965), 'Line Broadening', in Huddlestone R H and Leonard S L (eds), *Plasma Diagnostics Techniques*, New York, Academic Press, 265–317.

Wujec T, Janus H W and Jeleński W (2003), 'Spectroscopic measurements of electric field distributions in dielectric barrier discharges in hydrogen', *J. Phys. D: Appl. Phys.*, **36**, 868–877.